Pathological expansion of gut microbiome-associated *Enterococcus* in advanced cirrhosis corresponds with multilevel perturbations of the gut-liver-immune axis

Authors

Matthew J Dalby[1,2], Raymond Kiu[1,2], Marilena Stamouli[3], Betsy Arefaine[3], Lex E X Leong[4], Jack Hales[5], Christine Bernsmeier[6,7], Arjuna Singanayagam[8], Sidsel Støy[9], Maria-Emanuela Maxan[3], Merianne Mohamad[3], Ane Zamalloa[6], Matt Lewis[10], Royce P. Vincent[11,12], I. Jane Cox[3], Adrien Le Guennec[13], Roger Williams[3,19], Lindsey A Edwards[6], Shilpa Chokshi[15], Mark Thursz[10,16], Naiara Beraza[5], Charalambos G Antoniades[10,19], Debbie L Shawcross[3], Geraint B Rogers[4], Julia A Wendon[3], Kenneth D Bruce[17], *Lindsay J Hall[1,2,5,18], *Vishal C Patel[3,6]

Affiliations

1. Department of Microbes, Infection & Microbiomes, School of Infection, Inflammation and Immunology, College of Medicine & Health, University of Birmingham, Birmingham, UK.
2. Institute of Microbiology & Infection, University of Birmingham, Birmingham, UK.
3. Roger Williams Institute of Liver Studies, School of Immunology & Microbial Sciences, Faculty of Life Sciences and Medicine, King's College London, Foundation for Liver Research and King's College Hospital, London, UK
4. Infection & Immunity Theme, South Australian Health & Medical Research Institute, North Terrace, Adelaide, SA, Australia.
5. Food, Microbiome and Health, Quadram Institute Bioscience, Norwich Research Park, Norwich, UK.
6. Institute of Liver Studies, King's College Hospital NHS Foundation Trust, London, United Kingdom
7. Department of Biomedicine, University of Basel, Switzerland.
8. Infection Clinical Academic Group, St. George's School of Health and Medical Sciences, City St. George's University of London, Cranmer Terrace, London, SW17 0RE, UK.
9. Department of Hepatology and Gastroenterology, Aarhus University Hospital, DK-8200 Aarhus, Denmark.
10. Division of Digestive Disease, Department of Metabolism, Digestion & Reproduction, Imperial College London, London, UK.
11. Department of Clinical Biochemistry, King's College Hospital NHS Foundation Trust, London, UK;
12. Department of Nutritional Sciences, Faculty of Life Sciences and Medicine, King's College London, London, UK
13. Randall Centre for Cell & Molecular Biophysics and Centre for Biomolecular Spectroscopy, King's College London, London SE1 1UL, UK

14. Centre for Host-Microbiome Interactions, Faculty of Dentistry, Oral & Craniofacial Sciences, King's College London, SE1 9RT, UK
15. Faculty of Health, University of Plymouth, Devon, UK
16. Imperial College Healthcare NHS Trust, St Mary's Hospital, Praed St, London, UK.
17. Institute of Pharmaceutical Science, King's College London, UK.
18. Norwich Medical School, University of East Anglia, Norwich Research Park, Norwich, UK.
19. *In memoriam.*

* Joint last and corresponding authors.

Keywords: cirrhosis; advanced chronic liver disease; acute-on-chronic liver failure; microbiota; microbiome; *Enterococcus*; bile acids, bacterial translocation, gut inflammation, systemic inflammation, monocyte dysfunction

Funding statement: The observational study was adopted to the National Institute for Health Research (NIHR) Clinical Research Network (CRN) portfolio, supporting participant screening and recruitment by the Liver Research and Anaesthetics, Critical Care, Emergency and Trauma Teams at King's College Hospital NHS Foundation Trust. VCP was supported by a New Investigator Award from the Intensive Care Foundation (Registered charity number: 2940178) and Clinical Research Network South London Principal Investigator Strategic "GreenShoot" Research Delivery and Development Funding. The RIFSYS clinical trial was funded through an investigator-initiated study grant awarded by Norgine Pharmaceuticals UK Limited to King's College London. Infrastructure to support the trial was also provided by the Medical Research Council (MRC) Centre for Transplantation, King's College London, UK – MRC grant no. MR/J006742/1. Laboratory assays were also part funded by a generous donation from a Liver Service User to the King's College Hospital Institute of Liver Studies and Transplantation Charity Research Fund, King's College Hospital Charity (Registered charity number: 1165593). MS, BA, MEM, MM, IJC, SC and VCP were supported and bioinformatic analyses were part funded by the Foundation for Liver Research (Registered charity number: 268211/1134579). LJH is supported by Wellcome Trust Investigator Award (220876/Z/20/Z); the Biotechnology and Biological Sciences Research Council (BBSRC), Institute Strategic Programme Gut Microbes and Health (BB/R012490/1), and its constituent projects BBS/E/F/000PR10353 and BBS/E/F/000PR10356, and the BBSRC Institute Strategic Programme Food, Microbiome and Health BB/X011054/1 and its constituent project BBS/E/QU/230001B. MT Acknowledges support from the NIHR-Imperial

64 Biomedical Research Centre and the Medical Research Council Precision Medicine Award
65 (MR/R014019/1).

66

Conflicts of interest:

LAE has undertaken consultancy for EnteroBiotix.

DLS has undertaken consultancy for Norgine Pharmaceuticals Ltd, EnteroBiotix, MRM Health, Apollo Therapeutics, Genfit and Satellite Biosciences.

RPV reports Honoraria from Novo Nordisk, Amarin UK and AstraZeneca.

AS has delivered paid lectures for Bristol Myers Squibb.

VCP has undertaken consultancy for Norgine Pharmaceuticals Ltd, Alfasigma S.p.A., AstraZeneca and Menarini Diagnostics Ltd.

MD, LH, RK, IJC, ALG, GR, SS, SC, KB have no conflicts.

Authors contributions:

- Matthew J Dalby: Data curation, Formal analysis, Investigation, Software, Visualisation, Writing - Original Draft, Writing - Review & Editing
- Raymond Kiu: Data curation, Formal analysis, Writing - Review & Editing
- Marilena Stamouli: Data curation, Formal analysis, Writing - Review & Editing
- Betsy Arefaine: Data curation, Formal analysis
- Lex E X Leong: Data curation, Formal analysis, Investigation, Visualization, Writing - Review & Editing
- Jack Hales: Methodology, Writing - Review & Editing
- Christine Bernsmeier: Data curation, Formal analysis, Visualization, Writing - Review & Editing
- Arjuna Singanayagam: Data curation, Formal analysis, Visualization, Writing - Review & Editing
- Sidsel Støy: Data curation, Formal analysis, Visualization, Writing - Review & Editing
- Maria-Emanuela Maxan: Data curation, Writing - Review & Editing
- Merianne Mohamad: Visualization, Writing - Review & Editing
- Matt Lewis: Investigation, Methodology, Writing - Review & Editing
- Royce P Vincent: Resources, Writing - Review & Editing
- Jane Cox: Data curation, Formal analysis, Investigation, Visualization, Writing - Review & Editing
- Adrien Le Guennec: Data curation, Visualization, Writing - Review & Editing
- Roger Williams: Supervision
- Lindsey A Edwards: Data curation, Formal analysis, Writing - Review & Editing

- Shilpa Chokshi: Supervision, Writing – review & editing
- Mark Thursz: Resources, Supervision, Writing – review & editing
- Naiara Beraza: Investigation, Resources, Writing - Review & Editing
- Charalambos G Antoniades: Supervision
- Debbie L Shawcross: Conceptualisation, Funding acquisition, Resources, Supervision, Writing – review & editing, served as Chief Investigator of RIFSYS Trial
- Geraint B Rogers: Conceptualisation, Data curation, Formal analysis, Investigation, Resources, Supervision, Visualization, Writing - Review & Editing
- Julia A Wendon: Conceptualisation, Supervision, Writing – review & editing
- Kenneth D Bruce: Conceptualisation, Supervision, Writing – review & editing
- Vishal C Patel: Conceptualisation, Funding acquisition, Investigation, Methodology, Project administration, Resources, Supervision, Writing – review & editing, served as Chief Investigator of GLA study
- Lindsay J Hall: Conceptualisation, Funding acquisition, Investigation, Methodology, Project administration, Resources, Supervision, Writing – review & editing

Data availability:

The 16S rRNA amplicon sequencing raw reads are deposited in NCBI SRA under project PRJNA1223169.

Abstract

Background: Chronic liver disease (CLD) is a progressive condition that can advance to cirrhosis and acute-on-chronic liver failure (ACLF), a syndrome characterised by multi-organ dysfunction, critical illness, and high mortality. ACLF is driven by systemic inflammation, often without overt infection, suggesting alternative immune activation pathways, including microbial translocation. While intestinal perturbations, bacterial translocation, and immune dysfunction are hallmarks of ACLF, the specific microbial contributors remain unclear.

Objective: To investigate relationships between gut microbiome alterations, systemic inflammation, and clinical markers of disease severity across the cirrhosis spectrum.

Design: This cross-sectional, prospective study analysed faecal microbiota, plasma bile acids, urinary and plasma metabolites, gut and systemic inflammation and translocation markers, and monocyte dysfunction, in a well-phenotyped cohort of ACLF patients, decompensated and stable cirrhosis, compared to healthy individuals.

Results: Advanced stages of cirrhosis exhibited higher *Enterococcus* abundance, correlating with systemic inflammation, particularly in ACLF patients. Anaerobic commensal genera (*Roseburia*, *Ruminococcus*, and *Faecalibacterium*) were significantly lower. Lower urinary hippurate and trimethylamine N-oxide (TMAO) levels, linked to reduced microbial metabolism, paralleled these microbiome changes. Systemic inflammatory markers suggested parallel gut barrier dysfunction and microbial translocation in advanced cirrhosis.

Conclusion: Intestinal *Enterococcus* abundance, in advanced cirrhosis with greater antibiotic exposure, is a potential driver of gut barrier inflammation and dysfunction, and systemic immune activation. Further research into tailored microbiome-targeted therapies, including prebiotics, probiotics, phages and focused antibiotic use may prevent *Enterococcus* dominance, restore gut-liver axis homeostasis, and mitigate disease progression in cirrhosis.

Graphical Abstract

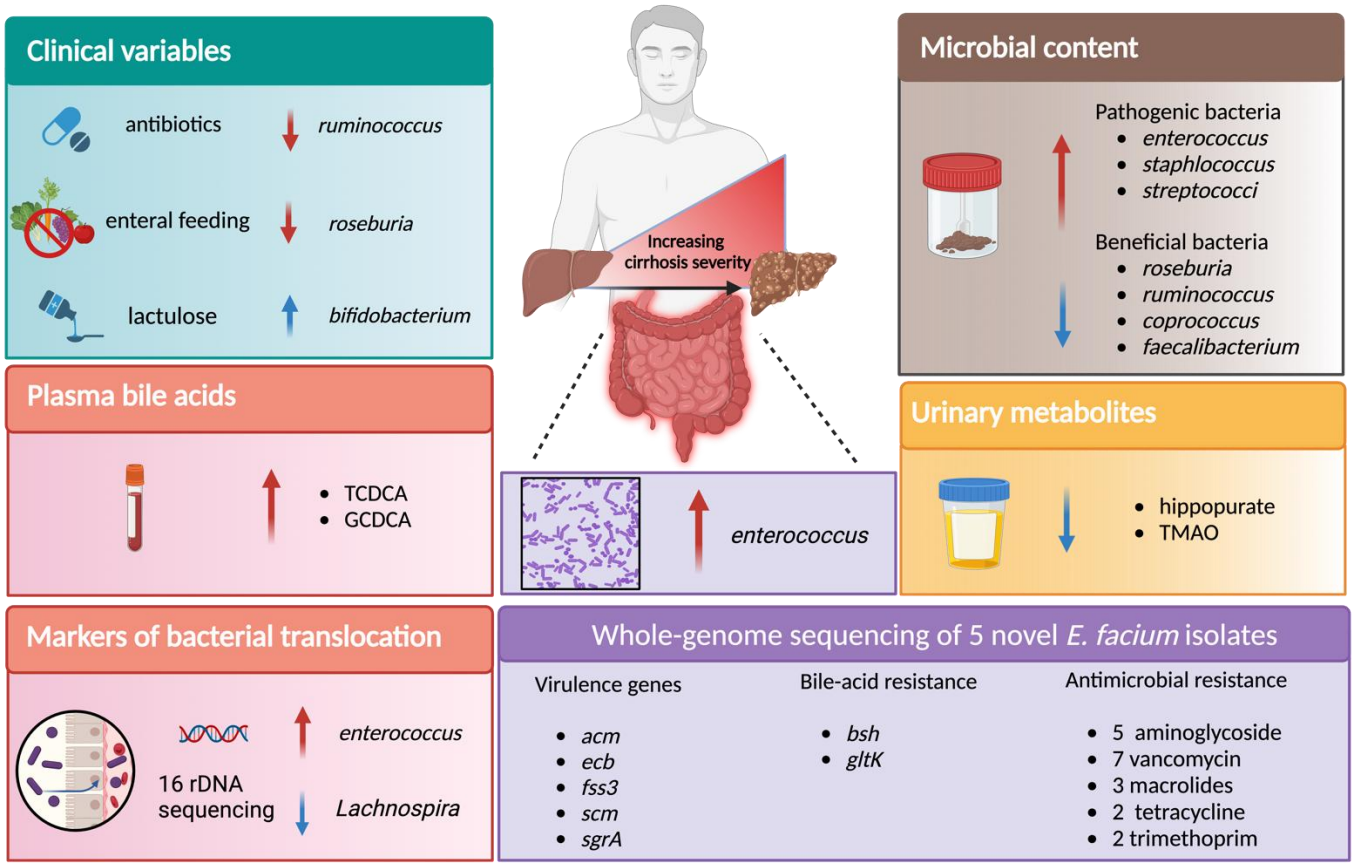

142 # Key messages

143 **What is already known on this topic**:

144 - CLD can progress to ACLF, a life-threatening syndrome with high mortality rates characterised
145 by systemic inflammation, impaired phagocytosis and immune dysfunction with associated
146 multiple organ failure.
147 - The gut microbiome's role in underpinning the gut-liver axis is recognised, with microbial
148 perturbations and gut barrier dysfunction associated with CLD, yet the exact microbiome
149 changes and their link to inflammatory pathways remain unclear.

150 **What this study adds:**

151 - This study reveals that *Enterococcus* significantly increases with CLD severity and antibiotic
152 use and correlates with markers of systemic inflammation and gut barrier dysfunction.
153 - Reductions in obligate anaerobe commensal bacteria, such as *Roseburia* and
154 *Faecalibacterium*, are observed, alongside depressed levels of key microbial metabolites,
155 including hippurate and TMAO, across CLD stages.
156 - These changes suggest that *Enterococcus* predominance and gut microbiome perturbations
157 driven by factors including disease severity and antibiotic use may actively drive inflammation
158 and impaired monocyte function in CLD.

159 **How this study might affect research, practice, or policy**:

160 - Findings indicate that *Enterococcus* and wider gut microbiome perturbations provide a
161 rationale for targeting as therapeutic strategies to modulate the gut-liver axis in CLD.
162 - This highlights the potential of microbiome-focused interventions, such as faecal microbial
163 transplantation, probiotics, prebiotics or phages, to improve gut health, reduce gut and
164 systemic inflammation, and ultimately mitigate cirrhosis-related complications.
165 - Future research and development of targeted microbiome therapeutics and rapid infection
166 diagnostics may positively influence CLD management, including a focus on antimicrobial
167 stewardship and informing clinical guidelines whilst improving patient outcomes.

1. Introduction

Chronic liver disease (CLD) is a progressive condition, resulting from several different aetiologies such as alcohol, viral hepatitis, and obesity that can culminate in cirrhosis and eventual liver failure (Huang et al., 2023). An important aspect of CLD is the development of acute-on-chronic liver failure (ACLF), a distinct syndrome characterised by multi-organ dysfunction, worsening liver function, and liver failure, with high mortality rates (Katoonizadeh et al., 2010; Moreau et al., 2013; Shah et al., 2024). The transition to decompensated cirrhosis, preceding ACLF, can lack identifiable triggers, confounding therapeutic options, exacerbating morbidity, and reducing transplant-free survival (D'Amico et al., 2022; Trebicka et al., 2021).

The gut microbiota is a key component of the 'gut-liver axis' but its interplay with the disease mechanisms is still not fully understood in CLD (Albillos et al., 2020; Hsu and Schnabl, 2023). While bacterial infections can act as a trigger of progression to ACLF, many cases (60-70%) display systemic inflammation without identifiable infection, with 50% of patients with 'sepsis' culture negative, suggesting alternative inflammatory pathways and limitations in infection diagnosis methods (Hernaez et al., 2017; Toledo et al., 1993). This 'sterile inflammation' in CLD patients may be driven by damage-associated molecular patterns (DAMPs) released from stressed or dying hepatocytes particularly in those without clear triggers such as active alcohol use or culture-confirmed bacterial infections (Arroyo et al., 2015). Additionally, translocation of viable bacteria or microbial components (i.e., microbial-associated molecular patterns [MAMPs]) *via* a dysfunctional intestinal barrier, may contribute to systemic inflammation, precipitating cirrhosis-related complications. Increased markers of gut permeability and inflammation in CLD patients further support the link between microbial translocation and inflammatory responses (Alexopoulou et al., 2017; Riva et al., 2020).

The gut microbiota potentially plays a dual role in CLD, serving as a reservoir for pathogens and MAMPs, while also simultaneously maintaining gut homeostasis through its resident commensal bacteria (Adak and Khan, 2019; Caballero-Flores et al., 2023). These commensal anaerobic microbes are critical for intestinal epithelial integrity, pathobiont exclusion (and preventing overgrowth), and metabolite production (e.g. short-chain fatty acids [SCFAs]) essential for host health (Ghosh et al., 2021). In CLD, however, gut microbiota disruptions are frequently observed, associated with reduced

196 intestinal barrier integrity, leading to disrupted mucosal immune priming and increased microbial
197 translocation. This process introduces intestinal bacteria and MAMPs into the systemic circulation,
198 contributing to cirrhosis-related inflammation, particularly in advanced disease stages. Studies in CLD
199 have reported reductions in commensal bacterial genera such as *Ruminococcus, Faecalibacterium,*
200 *Bacteroidetes,* and *Coprococcus* (Da Silva et al., 2018; Dubinkina et al., 2017), accompanied by
201 increases in pathobiont taxa like *Enterococcaceae*, *Staphylococcaceae*, and *Enterobacteriaceae* (Bajaj
202 et al., 2014). Additionally, patients with CLD show altered bile acid homeostasis, characterised by
203 alterations in bile acid quantities and composition, which correlate with microbiota shifts and
204 reduced conversion of primary to secondary bile acids (Kakiyama et al., 2013; Mouzaki et al., 2016),
205 with more primary bile acids being found in faeces (Kakiyama et al., 2014). These changes, mirrored
206 in serum bile acids, worsen with cirrhosis progression (Horvatits et al., 2017). However,
207 comprehensive studies integrating microbiota alterations to systemic metabolites, inflammatory and
208 gut barrier markers, across CLD stages remain limited. (Bajaj et al., 2022, 2014, 2012).

209 This study aimed to identify alterations in bacterial genera in the faecal microbiota, as targets for
210 future therapeutic intervention, across a well-phenotyped cohort of patients with ACLF,
211 decompensated cirrhosis, stable cirrhosis, and compared to healthy controls. We aimed to
212 understand some of the potential functional properties in these microbiome changes by comparison
213 with profiling of serum bile acids, urinary and plasma metabolites, and markers of gut inflammation,
214 bacterial translocation and systemic immune activation, as key pathobiological processes within the
215 gut-liver-immune axis. We hypothesised that microbiota perturbations increase with CLD severity.
216 By correlating these microbiota differences with relevant metabolic, inflammatory, immunological
217 and clinical disease markers, we aimed to detect key target bacteria within the gut that are associated
218 with disruption within the gut-liver-immune axis, providing insights into disease pathobiology and
219 informing potential therapeutic targets.

220 # 2. Results

221 **2.1 Participant characteristics**

222 This cross-sectional cohort included patients with cirrhosis who were categorised based on disease
223 stage and severity; stable cirrhosis (SC), decompensated cirrhosis (DC), or acute-on-chronic liver
224 failure (ACLF). A healthy control (HC) group of healthy participants was included for comparison
225 analysis and to establish normal values. Table 1 summarises demographic, clinical and biochemical
226 characteristics of the recruited patients and healthy controls. A total of 153 patients with cirrhosis
227 were included in this study (SC=15, DC=81, ACLF=57) with 40 HCs. Patients with cirrhosis were older
228 than HC with a mean HC age of 36 years (SD: 10 years) and mean liver cohort age of 53 years (SD: 11
229 years). Predominant aetiologies of cirrhosis included alcohol-related liver disease (ARLD)
230 (SC/DC/ACLF: 60%/70.4%/57.9%) and metabolic- dysfunction associated steatotic liver disease
231 (MASLD) (SC/DC/ACLF: 20%/8.6%/10.5%), respectively. SC, DC and ACLF patients presented with
232 ascites (33.3%/71.6%/96.5%) and HE (6.7%/43.2%/86%) as predominant manifestations of hepatic
233 decompensation, respectively. None of the cirrhosis patients had experienced a variceal
234 haemorrhage in the 7 days prior to recruitment nor had spontaneous bacterial peritonitis at the time
235 of sampling. DC and ACLF patients were more frequently receiving antibiotics acutely 45.7%/91.2%,
236 respectively) compared to SC (20%). There was no difference in use of rifaximin-α (only five
237 participants received rifaximin-α monotherapy as antibiotic treatment), lactulose, non-selective
238 beta-blockers and acid suppression therapies (proton pump inhibitors, H2 antagonists) across the
239 cirrhosis cohorts. Haematological, biochemical and disease severity and prognostic composite scores
240 followed expected patterns. Transplant-free survival at 90 days was 77.8% and 24.6% for the DC and
241 ACLF groups, respectively, with no deaths observed in the SC group.

242 **2.2. Microbiota diversity, bacterial translocation, faecal calprotectin, serum bile acid, and**
243 **metabolites profiles are progressively altered with increasing cirrhosis severity.**

244 Initial analysis focused on the composition of the faecal microbiota, plasma bile acids, urinary
245 metabolites and serum metabolites between cirrhosis severity groups in comparison to HCs. Faecal
246 microbiota diversity, both the number of bacterial genera detected (**Figure 1A)** and the Inverse

247 Simpson diversity index (**Figure 1B**), was lower in patients with more advanced cirrhosis compared
248 to all other groups. Clustering analysis using non-metric multidimensional scaling (NMDS) shows
249 separation in gut microbiota composition between ACLF and HC, with DC clustered between HC and
250 ACLF, while SC clustered closely to HC (**Figure 1C; Supplementary File 2**). The overall effect of disease
251 severity was tested using a PERMANOVA test (R2 = 13.5%; P = 0.0001) and a pairwise comparison
252 showed that the ACLF group clustered separately ($P < 0.05$) from DC, SC, and HC groups with DC also
253 different to the HC group (**Supplementary File 6**). To assess the associations between clinical
254 metadata variables, NMDS analysis was specifically conducted on faecal sequencing data from
255 patients with cirrhosis excluding HCs. Envfit analysis was used to examine the influence of 69 clinical
256 variables on microbiota composition. Forty-one clinical variables were significantly associated with
257 microbiota composition in patients with cirrhosis, with measures of cirrhosis severity exhibiting the
258 most pronounced impact (**Supplementary Figure 1A; Supplementary File 7**). For the purposes of
259 visualisation the ten clinical variables with the highest R2 values with the strongest association with
260 the microbiota composition were overlaid on the NMDS plot and were all correlated with cirrhosis
261 severity (**Supplementary Figure 1B; Supplementary File 7**).

262 NMDS plots comparing plasma bile acid composition indicated higher divergence amongst HC
263 samples, and an increasing convergence (clustering) with cirrhosis severity (PERMANOVA: P=0.0001)
264 (**Figure 1D; Supplementary File 3,6**). Both urine (PERMANOVA: P=0.0001) and plasma metabolites
265 (PERMANOVA: P=0.0001) showed significant separation in clustering based on cirrhosis severity with
266 similar NMDS clustering with tightly clustered HC samples and divergent cirrhosis patient samples,
267 particularly for ACLF (**Figure 1E-F; Supplementary File 6**). Multivariate analysis, after obvious
268 exclusions including for dominant glucose or ethanol peaks, for example, showed separation of the
269 four study cohorts (HC, n=36; SC, n=8; DC, n=67; and ACLF, N=36) with pairwise multilevel comparison
270 showing significant differences between all groups except SC and DC ($P < 0.05$). This was also
271 confirmed visually by the NMDS plots (**Figure E; Supplementary File 5**) and relative metabolite levels
272 per grouping for TMAO, hippurate (**Figure 3F; Supplementary File 6**) and for creatinine, citrate,
273 dimethylamine, formate and mannitol (**Supplementary Figure 3**).

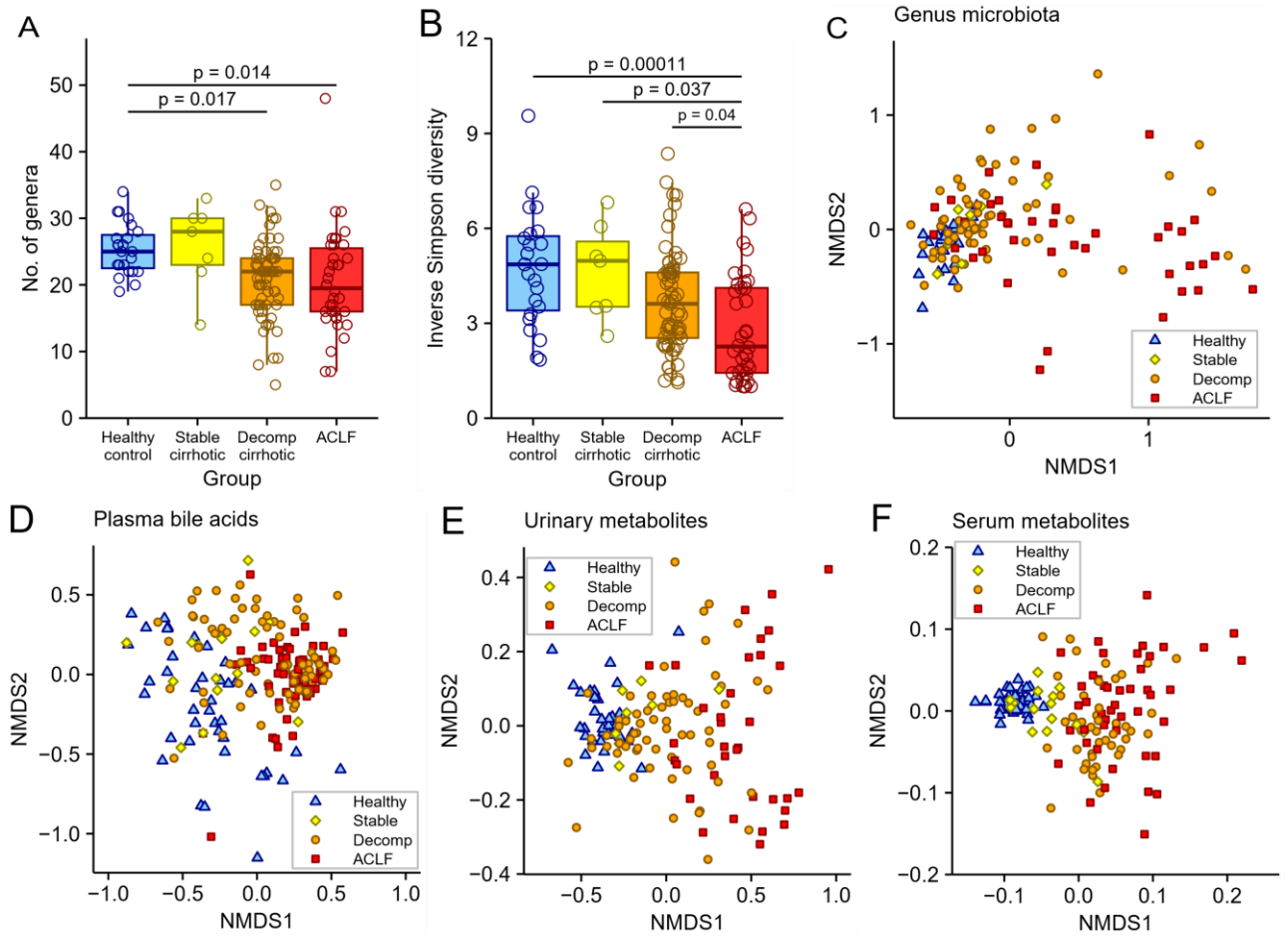

Figure 1: Comparison of faecal microbiota diversity, plasma bile acids, and metabolites profiles in cirrhosis and healthy controls.

(A) Number of genera detected in each participant's faecal sample by cirrhosis severity and HC. (B) Faecal microbiota diversity measured using the Inverse Simpson diversity index by cirrhosis severity vs HC. NMDS ordination shows dissimilarity indices via Bray-Curtis distances between individual participants coloured by cirrhosis severity vs HC (D) plasma bile acids (E) urinary metabolites and (F) serum metabolites. Dot and box plots show median and interquartile ranges of data with circles showing each individual participant.

2.3. Genus-level microbiota composition at different cirrhosis severities reveals a progressive overabundance of *Enterococcus* with reductions in commensal taxa.

285 To investigate alterations in gut microbiota composition in more detail, bacterial genus profiles
286 within individual participants were examined. Stacked bar plots showing the ten most abundant
287 bacterial genera illustrate an increasing dominance of *Enterococcus* in more advanced cirrhosis i.e.
288 DC and ACLF groups (**Figure 2A**). Differential abundance of bacterial genera is represented in a heat
289 map showing significant associations between faecal bacterial genera comparing the three cirrhosis
290 groups with HC (**Figure 2B; Supplementary file 8**). *Ruminococcus, Roseburia,* and *Lachnospira*
291 showed the strongest negative association with cirrhosis severity with the lowest abundances in ACLF
292 and DC patients compared to HC (**Figure 2C-E**). *Enterococcus* and *Staphylococcus* showed the
293 strongest positive association with cirrhosis severity with highest abundance in ACLF relative to HC
294 (**Figure 2FH**), while *Streptococcus* abundance was higher in DC and SC compared to HC (**Figure 2G)**.
295 *Enterococcus* abundance was markedly higher in the ACLF patient group compared to HC (**Figure 2C)**.
296 Conversely, a proportion of more severely ill patients with cirrhosis have gut microbiota dominated
297 by *Enterococcus*, with significantly elevated levels observed in DC and ACLF. In a quarter of ACLF
298 patients, the relative abundance of *Enterococcus* exceeded 75%.

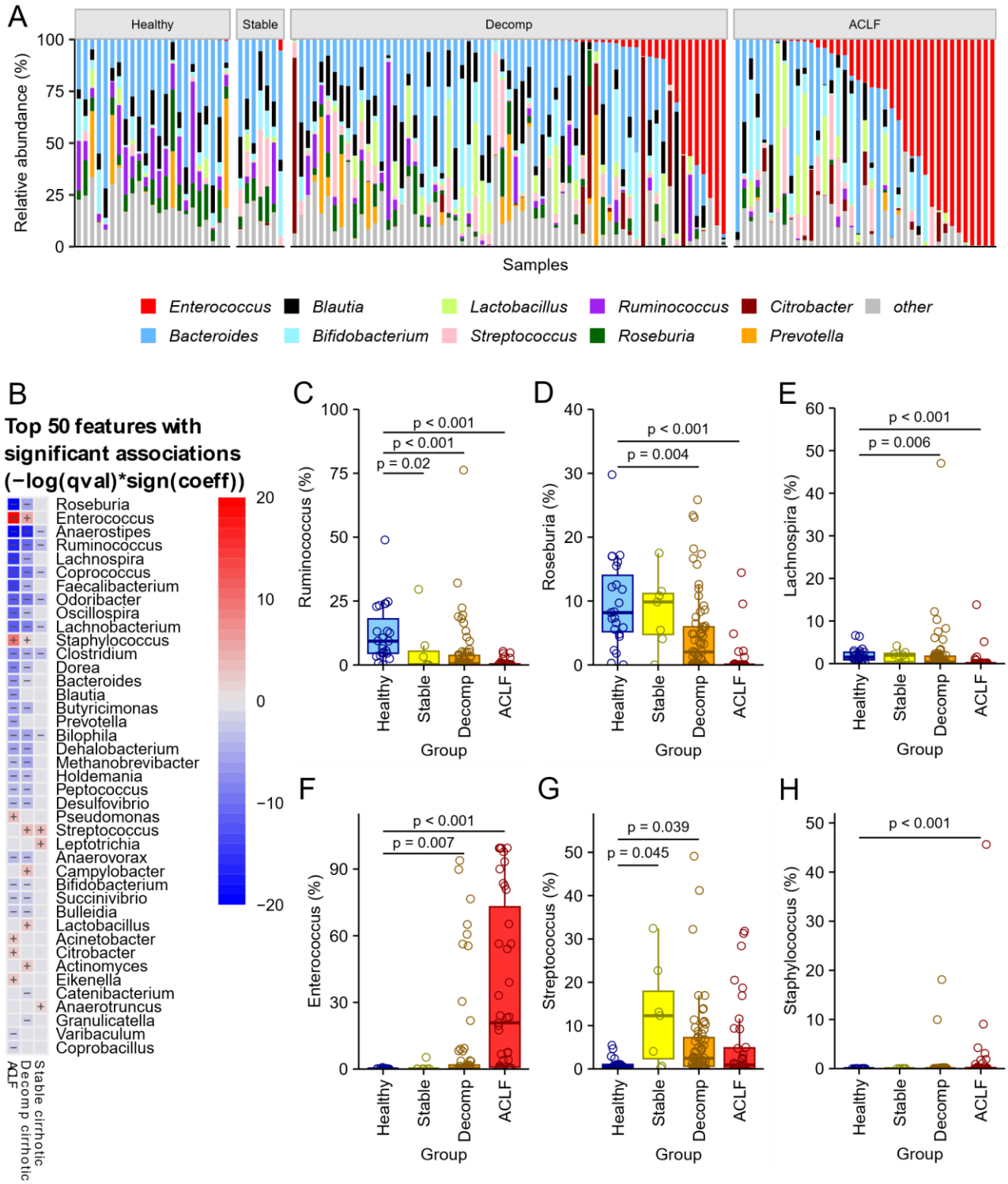

Figure 2: Microbiota genus composition in cirrhosis vs. healthy controls.

(A) Stacked bar plots show the ten most abundant bacterial genera in faecal samples stacked by overall abundance, and with participants ordered within cirrhosis severity categories by proportion

303 of *Enterococcus*. (B) The heat map displays MaAslin2 analysis of significant associations between
304 faecal genus abundance and cirrhosis severity with HC used as a reference. The three genera with
305 the strongest negative effect size for cirrhosis severity determined by MaAslin2 using HC as a
306 reference and shown as box and dot plots were (C) *Ruminococcus*, (D) *Roseburia*, and (E) *Lachnospira*.
307 The three genera with the strongest positive effect size for cirrhosis severity determined by MaAsLin2
308 using HC as a reference and shown as box and dot plots were (F) *Enterococcus*, (G) *Streptococcus*,
309 and (H) *Staphylococcus*. Dot and box plots show median and interquartile ranges of data with circles
310 showing each individual participant.

311 **2.4. Plasma bile acids and urinary metabolites correlate with specific gut microbiota taxa with**
312 **increasing cirrhosis severity.**

313 To determine the impact of cirrhosis severity on alterations in plasma bile acids, urinary metabolites,
314 and serum metabolites, we correlated these, using MaAsLin2, with faecal bacterial genera to
315 investigate their associations with gut microbiota composition and provide putative insights into
316 alterations in microbiome function. The primary bile acids taurochenodeoxycholic acid (TCDCA),
317 glycochenodeoxycholic acid (GCDCA), taurocholic acid (TCA) and glycocholic acid (GCA) were higher
318 in the plasma of patients with cirrhosis compared to HC, while other bile acids were lower than in HC
319 (**Figure 3A; Supplementary File 9**). TCDCA and GCDCA showed the strongest effect size with higher
320 concentrations in all three cirrhosis cohorts relative to HC (**Figure 3B-C; Supplementary Figure 3**).
321 Contrasting plasma bile acid concentrations with the percentage of bacterial genera showed that
322 *Enterococcus* abundance was positively correlated with primary bile acids including TCDCA, while
323 *Ruminococcus*, *Coprococcus*, and *Roseburia* were negatively correlated with primary bile acid
324 concentration (**Figure 3D; Supplementary Figure 2**).

325 Analysis of urinary metabolites showed several metabolites differing by cirrhosis severity relative to
326 HC (**Figure 3E; Supplementary File 10**). Two metabolites, hippurate (**Figure 3F**) and Trimethylamine
327 N-oxide (TMAO) (**Figure 3G**), were identified as products of gut microbial metabolism and both were
328 lower in patients with cirrhosis compared to HC, and lower in ACLF than in SC or DC (**Figure 3F-G**;
329 **Supplementary Figure 2**). Contrasting urinary metabolites with the percentage proportion of
330 bacterial genus showed that *Enterococcus* abundance was negatively correlated with several

331 metabolites including hippurate and TMAO, while *Ruminococcus*, *Coprococcus*, and *Roseburia* were
332 positively correlated with hippurate and TMAO (**Figure 3H; Supplementary Figure 3**).

333 Similar differences were seen in plasma metabolites with significant differences between cirrhosis
334 cohorts and HC (**Supplementary Figure 4A; Supplementary File 11**) amongst several plasma
335 metabolites (**Supplementary Figure 4B-G**). Similarly, *Enterococcus* abundance correlated with
336 changes in a number of plasma metabolites (**Supplementary Figure 4H**).

337 These findings show a pattern characterised by elevated concentrations of primary bile acids in
338 plasma and reduced quantities of recognised microbial metabolites in the urine among cirrhosis
339 patients with more advanced disease.

340

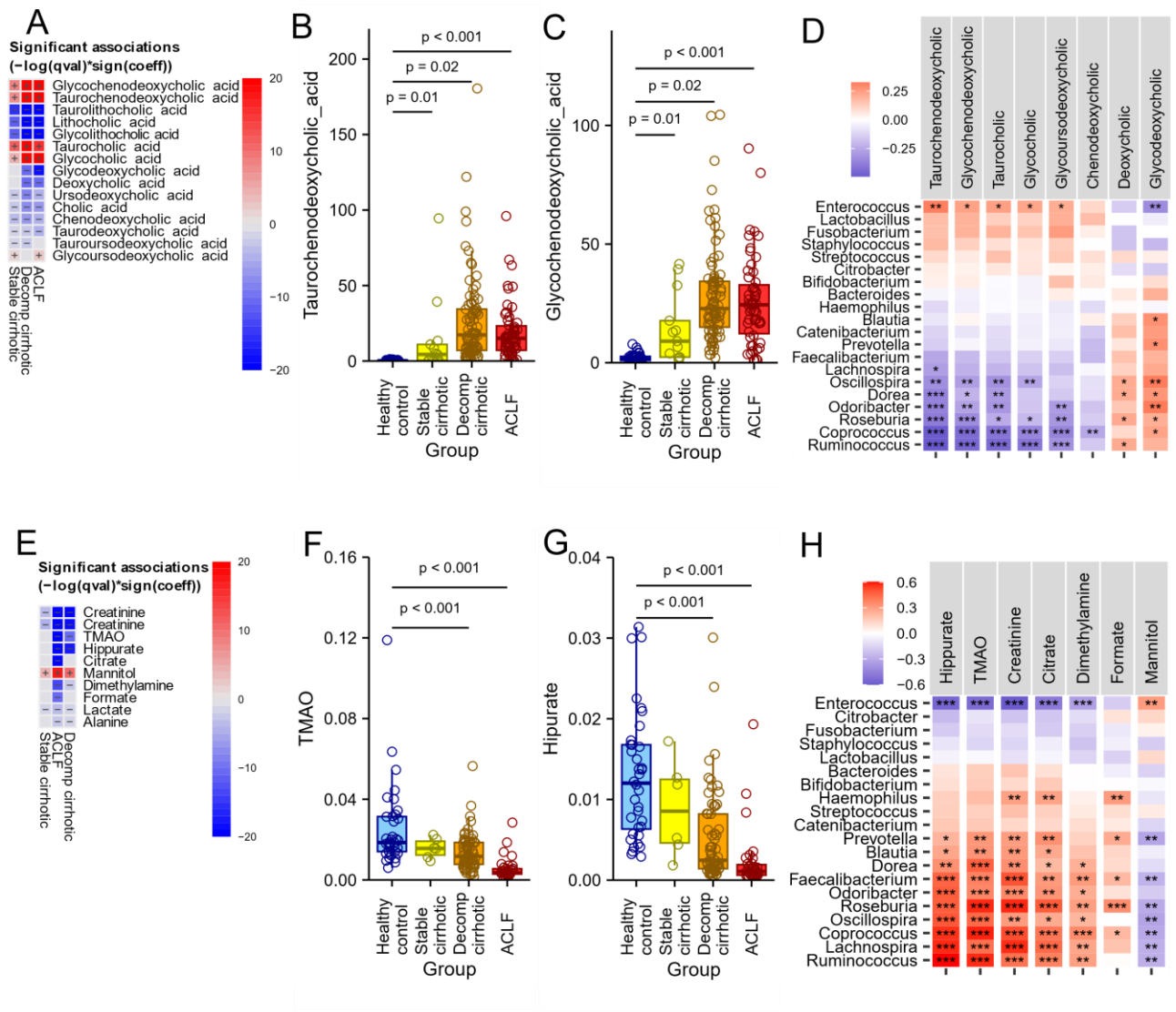

Figure 3: Plasma bile acids, urinary metabolites, and correlations with abundance of faecal bacterial genera.

(A) The heatmap displays MaAslin2 analysis results of significant associations between plasma bile acid concentrations and cirrhosis cohorts using HC as a reference. The two plasma bile acids with the strongest positive effect size for cirrhosis severity determined by MaAslin2 using HC as a reference and shown as box and dot plots were (B) Taurochenodeoxycholic acid and (C) Glycochenodeoxycholic acid. (D) Pearson correlations between the normalised relative abundance of the top twenty most abundant faecal bacterial genera (comprising 98% of the microbiota) and normalised plasma bile acid concentrations showing bile acids with significant correlations. (E) The heatmap displays MaAslin2

351 analysis results of significant associations between urinary metabolite concentrations and cirrhosis
352 severity using HC as a reference. The two urinary metabolites with the strongest negative effect size
353 for cirrhosis severity determined by MaAslin2 using HC as a reference and shown as box and dot plots
354 were (F) Trimethylamine N-oxide (TMAO) and (G) Hippurate. (H) Pearson correlations between the
355 normalised relative abundance of the top twenty most abundant faecal bacterial genera (comprising
356 98% of the microbiota) and normalised urinary metabolite concentrations showing metabolites with
357 significant ($P < 0.05$) correlations. Full correlations shown in Supplementary Figure 3 and 4.

358 **2.5. Clinical variables link to overall microbiota profiles, with further associations in advanced**
359 **cirrhosis of *Enterococcus* with antibiotic usage and resistance profiles**

360 Next, we carried out an exploratory analysis to determine how clinical parameters might be
361 associated with gut microbiota composition, using the envfit function, focusing on each clinical
362 variable and overall microbiota beta-diversity. The ten clinical variables with the strongest
363 association with faecal microbiota composition were plotted overlaying an NMDS plot
364 (**Supplementary Figure 1).** Several clinical factors correlated with microbiota composition, with
365 conventional measures of cirrhosis severity showing the strongest association (**Supplementary**
366 **Figure 1, Supplementary File 7**). Composite clinical scores are used to classify cirrhosis severity and
367 for prognostication. Of those included in this analysis, ACLF grade, MELD score, Child-Pugh grade and
368 score, and UKELD score were all associated with microbiota composition, in keeping with the study
369 phenotyping of the cirrhosis cohorts, i.e. SC, DC, and ACLF.

370 Antibiotic use, oral food intake, and lactulose use were clinical variables identified as both having an
371 association with microbiota composition, and considered likely to have a direct influence on the gut
372 microbiota **(Supplementary File 2)**. Differential abundance testing was carried out using MaAslin2
373 for antibiotic use, oral food intake, and lactulose use along with cirrhosis severity was included within
374 the MaAslin2 model to adjust for covariance (**Supplementary File 12**). Antibiotic use, oral food intake,
375 lactulose use, all showed significant effects on differential abundance of genus within the patient
376 cohort when adjusted for covariance. Comparing the genus with the large difference in abundance
377 in cirrhosis patients receiving or not receiving enteral intake, *Roseburia* abundance was lower in
378 patients not receiving nutrition *via* enteral routes (normal oral intake and by enteral tube feeding),

379 while *Enterococcus* abundance was higher (**Figure 4A**). Similarly, *Roseburia* abundance was lower in
380 patients receiving antibiotics, while *Enterococcus* abundance was higher (**Figure 4B**). Results were
381 unchanged when excluding the 5 patients only receiving rifaximin as antibiotic treatment. Lactulose
382 use was associated with a higher relative abundance of *Bifidobacterium* within the patient cohort
383 between those receiving lactulose and those not (Figure 4E). *Enterococcus* remained significantly
384 higher abundance in DC and ACLF severity groups compared to HC when adjusted for antibiotic use,
385 oral food intake indicating an independent effect of all three factors on *Enterococcus* abundance
386 (**Supplementary Table 2**).

387 The cirrhosis group as a whole received a total of 19 different types of antibiotics (**Figure 4F;**
388 **Supplementary Table 2.** The most frequently used antibiotics were piperacillin/tazobactam (Tazocin)
389 (33 patients) and 16 Meropenem (16 patients) totalling 37% of patients while 48 (36%) received no
390 antibiotics. The remaining 17 antibiotics were given to 6 or fewer patients with 8 antibiotics only
391 given to one patient. To visualise the complexities of this antibiotic administration, data was
392 visualised as a heatmap with patients clustered by antibiotic use and antibiotics clustered by co-
393 occurrence (**Figure 4C**). Associations of gut bacterial genus differential abundance with all individual
394 antibiotic administration was tested in a MaAslin2 model with only piperacillin/tazobactam (Tazocin)
395 and meropenem individually associated with abundance of *Enterococcus* (**Supplementary Table 8**
396 **Figure 4C**). Five out of 48 patients not currently receiving antibiotics also showed higher *Enterococcus*
397 relative abundance (**Figure 4C**). This cirrhosis cohort included a range of aetiologies, however,
398 aetiology did not influence gut microbiota composition. Rather, cirrhosis severity, antibiotic
399 exposure, and nutritional intake were the primary factors that co-associated with a dominant
400 *Enterococcus* gut microbiota signature in patients with the most severe disease i.e. DC and ACLF
401 (**Supplementary figure 7A,B**).

402 To probe *Enterococcus* traits in more detail, five isolates obtained from five different patient faecal
403 samples (one sample from the DC cohort and four from the ACLF cohort) underwent whole genome
404 sequencing and were identified as *Enterococcus faecium*. Comparing the similarities of these 5 novel
405 isolates with an additional publicly available 185 *E. faecium* genomes (retrieved from the NCBI
406 GenBank database) using midpoint rooted maximum-likelihood tree showed a diversity of *E. faecium*
407 genomes with no single clonal group colonising patients with cirrhosis indicating that the *E. faecium*

408 isolates did not originate from the same source (**Figure 4D**). The five *E. faecium* cirrhosis isolate
409 genomes were aligned against virulence-related gene profiles, antibiotic resistance genes, and bile
410 resistance genes (**Figure 4E**). These isolates contained between 12 and 17 of the 20 antibiotic
411 resistance genes analysed (**Figure 4E**); 5 genes encoding aminoglycoside resistance, 7 *van* genes
412 encoding vancomycin resistance, 3 encoding macrolides resistance, 2 encoding tetracycline
413 resistance, and 2 trimethoprim resistance. The two bile acid resistance genes *bsh* and *gltK* were
414 present in all patient isolates, and in the genomes of 95% of all 190 isolates from public databases
415 (**Figure 4F**).

416 Taken together, these data indicate that clinical factors such as reduced enteral nutritional intake
417 and exposure to the broad-spectrum beta-lactam antibiotics piperacillin/tazobactam (Tazocin) and
418 meropenem were strongly linked to higher levels of *Enterococcus* and decreased abundance of
419 commensal genera in patients with cirrhosis. Broad-spectrum beta-lactam antibiotics are commonly
420 administered to DC and ACLF patients as part of their treatment regimen. *Enterococcus* isolates
421 obtained and sequenced from these patients were identified as *E. faecium* and were found to encode
422 various antibiotic and bile acid resistance genes, indicating potential bacterial survival mechanisms
423 and pathogenicity.

424

425

426

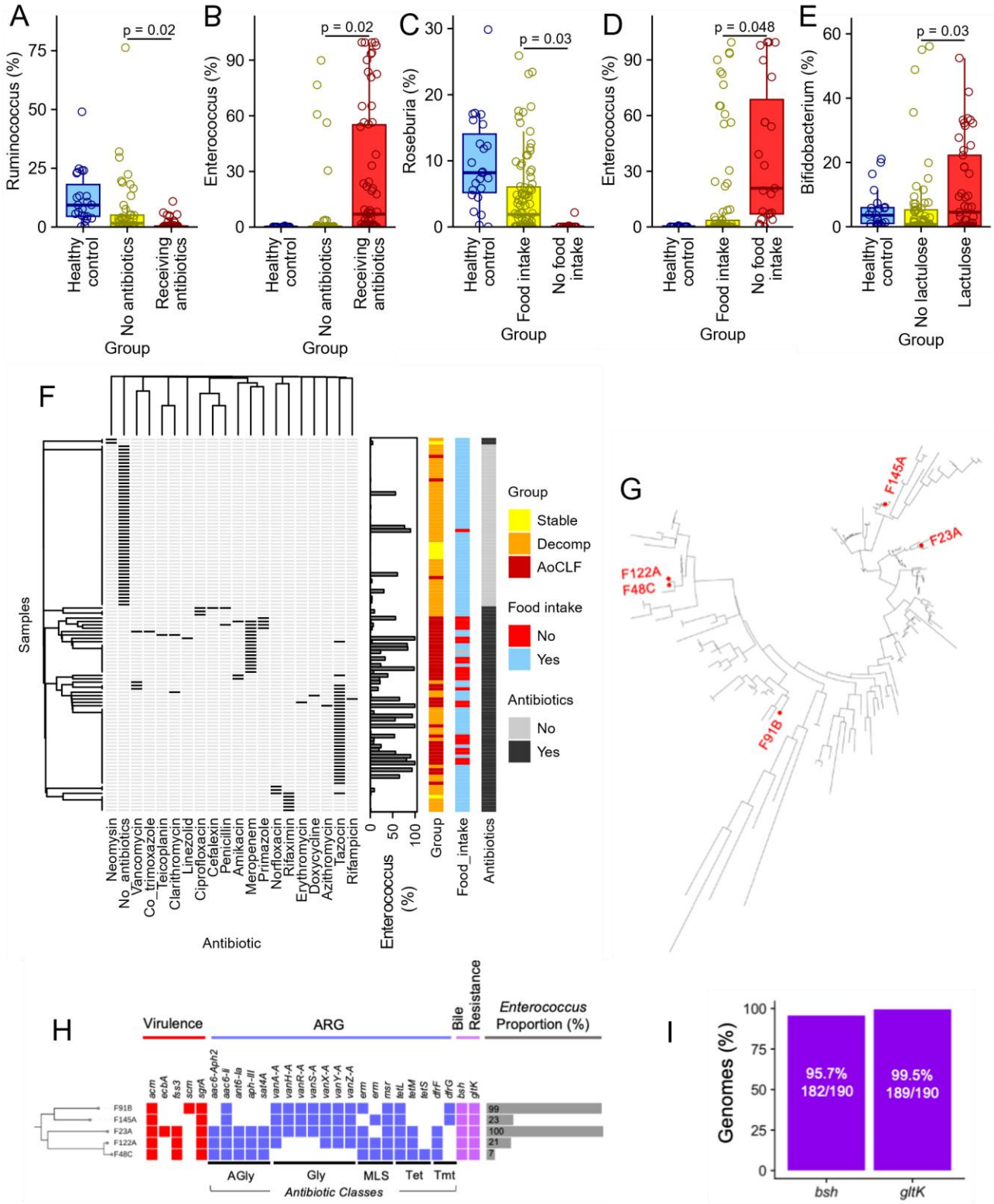

Figure 4: Oral food intake, receiving antibiotics, and *Enterococcus faecium* genomic data.

429 The differentially abundant genera with the strongest negative and positive effect sizes for antibiotics
430 with patients not receiving antibiotics as the reference were (A) *Ruminococcus* and (B) *Enterococcus*.
431 The differentially abundant genera with the strongest negative and positive effect sizes for nutritional
432 intake with patients not receiving enteral as the reference were (C) *Roseburia* and (D) *Enterococcus*.
433 The differentially abundant genera with the strongest positive effect size for lactulose use with
434 patients not receiving lactulose as the reference was (E) *Bifidobacterium*. (F) Clustered individual
435 antibiotics received by patients with cirrhosis cohort, nutritional status, and relative abundance of
436 *Enterococcus* in each sample. (G) A midpoint rooted maximum-likelihood tree consisted of 190
437 *Enterococcus faecium* genomes, including 5 novel *E. faecium* isolates obtained from cirrhosis
438 patients, as highlighted in the tree. (H) Novel *E. faecium* genomes (n=5) from cirrhosis patients
439 aligned with virulence-related gene profiles, virulence (using VFDB), ARG (Antibiotic Resistance
440 Genes; using ARG-ANNOT) and bile resistance genes (*bsh* and *gltK*), accordingly. Proportion of
441 *Enterococcus* (genus level; based on 16S rRNA sequence data) in the corresponding faecal samples
442 was also indicated in the horizontal bar chart. (I) Proportion of detectable bile resistance genes (%)
443 *bsh* and *gltK* in 190 *E. faecium* genomes, suggesting that these two genes belong to the core genome
444 of *E. faecium*.

445 **2.6. Faecal microbiota and markers of bacterial translocation, intestinal and systemic**
446 **inflammation, and monocyte exhaustion.**

447 To explore links between gut barrier dysfunction and translocation of intestinal bacteria and/or their
448 products from the gut into the systemic circulation, we determined the number of copies of 16S rDNA
449 in whole blood from cirrhosis patients and HC. The number of copies of 16S rDNA in the blood was
450 lowest in HC in keeping with a degree of 'physiological translocation' and displayed a stepwise
451 increase with severity of cirrhosis (**Figure 5A**). To identify associations with the faecal microbiota, we
452 correlated copies of 16S rDNA in the blood against percentages of bacterial genera (**Figure 5B**), with
453 *Enterococcus* most strongly positively correlated (**Figure 5C**), and *Lachnospira* most negatively
454 correlated (**Figure 5C**). Faecal calprotectin as a conventional marker of non-specific gut mucosal
455 inflammation also showed a stepwise increase with cirrhosis severity compared to HC (**Figure 5D**).
456 Faecal calprotectin was positively correlated with relative abundance of *Enterococcus* **(Figure 5E**) and
457 negatively correlated with *Lachnospira* (**Figure 5E**).

458 The innate immune function of CD14+ monocytes isolated from peripheral blood obtained from
459 cirrhosis patients and HCs was assessed by stimulation with TLR 2/4/9 agonists *in vitro*, with
460 unstimulated controls, and the percentage of Tumour necrosis factor-alpha (TNF- α), Interleukin-6
461 (IL-6), and monocyte human leukocyte antigen-DR (HLA-DR) positive monocytes identified by flow
462 cytometry. Monocytes from DC and ACLF patients showed attenuated proinflammatory responses
463 (TNF-α and IL-6) to Pam3, LPS and CpG challenge, indicating reduced innate responses to pathogen-
464 induced TLR signalling pathways. (**Supplementary Figure 1**). To identify cirrhosis-associated
465 alterations in monocyte function and associations with factors linked to the microbiota, the
466 percentage of TNF-α or IL-6 positive monocytes were correlated with copies of 16S rDNA in whole
467 blood, faecal calprotectin, and the twenty faecal genera with the highest overall abundance (**Figure**
468 **5I; Supplementary Figure 6**). The number of copies of bacterial DNA in whole blood positively
469 correlated with the percentage of IL-6 positive unstimulated monocytes, while the number of genera
470 positively correlated with the percentage of TNF- α and IL-6 positive LPS-stimulated monocytes
471 (**Figure 5I**). *Lachnospira* showed positive associations and *Enterococcus* negative associations with
472 the percentage of TNF- α and IL-6 positive LPS stimulated monocytes (**Figure 5J**) and *Enterococcus*
473 with TNF- α positive Pam3 stimulated monocytes (**Figure 5IK**).

474 These findings reveal contrasting associations between *Enterococcus* and other commensal bacterial
475 genera, such as *Lachnospira*, on markers of intestinal permeability, intestinal and systemic
476 inflammation, and monocyte innate immune function.

477

478

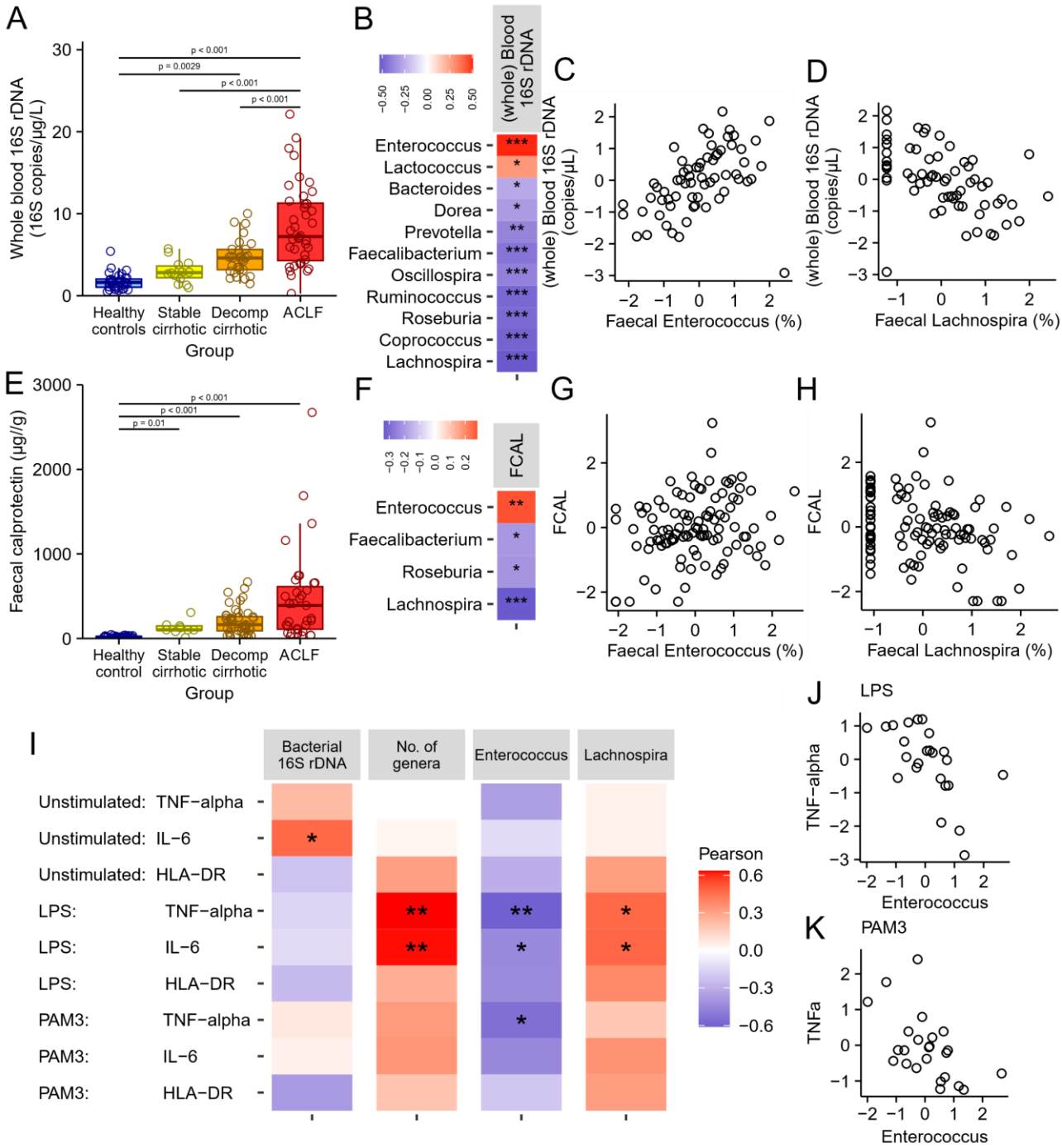

Figure 5. Markers of intestinal permeability and intestinal inflammation and correlations of stimulated monocyte activation with (whole) blood 16S rDNA and faecal microbiota.

(A) Copies of 16S rDNA in participant blood by cirrhosis severity vs HC. (B) Significant correlations between copies of 16S rDNA in participant blood and percentage of genera in the faecal microbiota. (C) Scatter plot of copies of 16S rDNA in blood against faecal *Enterococcus* for each participant. (D)

485 Scatter plot of copies of 16S rDNA in blood against faecal *Lachnospira* for each participant. (E) Faecal
486 calprotectin concentration by cirrhosis severity vs HC. (F) Significant correlations between faecal
487 calprotectin concentration and percentage of genera in the faecal microbiota. (G) Scatter plot of
488 faecal calprotectin concentration against faecal *Enterococcus* percentage for each participant. (H)
489 Scatter plot of faecal calprotectin concentration against faecal *Lachnospira* percentage for each
490 participant. (I) Percentage of monocytes showing TNF-α and IL-6 production and HLA-DR expression
491 in response to antigen stimuli (LPS/TLR-4; Pam3CSK4/TLR-2, CpG/TLR-9) correlated separately with
492 whole blood 16S rDNA, number of faecal genera, faecal *Enterococcus* percentage and faecal
493 *Lachnospira* percentage. Stars (*) indicate statistical significance ($P < 0.05$) after adjustment for
494 multiple testing. (J) Scatter plot of percentage of TNF- α positive LPS stimulated monocytes against
495 faecal *Enterococcus* percentage for each participant. (K) Scatter plot of percentage of TNF- α positive
496 PAM3 stimulated monocytes against faecal *Enterococcus* percentage for each participant.

497

498

499 # 3. Discussion

500 We found higher relative abundance of *Enterococcus* in the gut microbiota of patients with cirrhosis,
501 particularly in those with advanced disease and receiving broad spectrum antibiotics, accompanied
502 by a lower abundance of obligate anaerobic commensal genera. This shift is consistent with patterns
503 seen in other conditions with compromised intestinal barrier function, such as preterm infants
504 (Hufnagel et al., 2007) and Graft-versus-Host Disease (Garrett, 2020), as well as other studies in ACLF
505 (Lee et al., 2024a, 2024b; Solé et al., 2021). These findings suggest that *Enterococcus*, an
506 opportunistic pathogen, may exploit disrupted gut microbial communities and diminished
507 colonisation resistance to thrive, especially in advanced disease states with multiple gut microbiota
508 modulating treatments.

509 Multiple factors may contribute to the selection and proliferation of resident *Enterococcus* strains in
510 the gut of cirrhosis patients. Antibiotic use is one such factor, as many of the patients with high
511 *Enterococcus* levels had received broad-spectrum beta-lactam antibiotics like
512 Piperacillin/tazobactam or meropenem. These antibiotics are commonly administered to
513 hospitalised DC and ACLF patients for treating suspected infections, often before culture results are
514 available, and *Enterococcus* exhibits 100-fold less susceptibility to beta-lactam antibiotics (Zapun et
515 al., 2008), potentially providing a selective advantage. Additionally, the *E. faecium* isolates in this
516 study encoded genes conferring bile acid resistance (Zhang et al., 2013), which may further facilitate
517 persistence in the bile-rich environment characteristic of advanced cirrhosis (Kakiyama et al., 2013).
518 Elevated intestinal luminal bile acids in cirrhosis, particularly primary bile acids, can alter the gut
519 microbial environment (Ridlon et al., 2013), often reducing bile-sensitive commensals like *Roseburia*
520 and providing an ideal niche for *Enterococcus* to overgrow.

521 This relative overgrowth of *Enterococcus* in the gut microbiota, especially strains with virulence genes
522 like *acm* and *sgrA* (encoded in all strains isolated from this study cohort), which enhance adhesion
523 and translocation, presents significant clinical implications. These strains may be associated with
524 systemic infections that can exacerbate cirrhosis-related complications, such as progression from a
525 stable state to DC and ACLF (Hendrickx et al., 2009; Nallapareddy et al., 2008). Moreover, bacterial
526 sepsis is a significant complication in patients with cirrhosis, an increasing recognition of the threat

527 of antimicrobial resistance (Piano et al., 2019; Wong et al., 2021). Carriage of multidrug resistant
528 strains (as indicated by our genomic analysis) may contribute to greater clinical complication
529 episodes by way of hepatic decompensation, organ failure and mortality rates, due to increased
530 translocation of *Enterococcus* via a dysfunctional and inflamed gut barrier into the bloodstream.
531 Furthermore, as *Enterococcus* appears to dominate more severely ill patients to the exclusion of
532 other potential pathogens, this pattern raises questions about its source. Genomic analysis showed
533 divergent strains of *E. faecium* were present in patients rather than any common clonal lineages,
534 which would be the case if multiple patients had acquired the *E. faecium* from each other or from
535 the same hospital environment. This indicated that the *E. faecium* are more likely to represent
536 resident gut strains already in the patient rather than nosocomial infections. Further investigation
537 involving a larger number of isolates will be valuable to confirm these findings.

538 As faecal *Enterococcus* abundance increased, we observed a corresponding significant decline in key
539 commensal bacterial genera including *Roseburia*, *Ruminococcus*, *Coprococcus*, and *Faecalibacterium*,
540 with many ACLF patients showing an almost complete relative absence. These genera are essential
541 for SCFA production, such as butyrate (Flint et al., 2012), which supports intestinal barrier integrity.
542 The loss of these beneficial microbes is a common feature in cirrhosis (Acharya and Bajaj, 2019) that
543 is linked to the development of gut barrier failure, pathological microbial translocation and cirrhosis-
544 associated immune dysfunction. Their decline appears to be further exacerbated by common
545 therapeutic factors in the treatment of advanced cirrhosis, such as the use of broad-spectrum
546 antibiotics, which impact antibiotic-sensitive species (Zimmermann and Curtis, 2019), and a reliance
547 on fibre-deficient diets, particularly among patients dependent on enteral or parenteral nutrition
548 (present in 45% of the ACLF group). These diets lack the necessary fermentable dietary fibre to
549 sustain SCFA-producing microbes, worsening microbial disruption and potentially contributing to gut
550 permeability.

551 This microbiota disruption is mirrored by lower urinary levels of metabolites like hippurate which is
552 a products of beneficial microbial metabolism and fibre-rich diets (Lees et al., 2013) and TMAO, which
553 is a microbial byproduct of metabolising nutrients including choline, betaine, and carnitine found in
554 meat, eggs, and fish (Pallister et al., 2017). Hippurate production, often associated with microbial
555 metabolism of phenolic compounds in fruits and vegetables, was positively correlated with

556 *Ruminococcus*, further linking microbial loss with decreased metabolic activity. Similarly, TMAO -
557 produced via hepatic conversion of trimethylamine (TMA), itself a microbial metabolite from dietary
558 sources like carnitine and lecithin - was also reduced, indicating either a reduction in dietary
559 substrates or a loss of the bacteria producing TMA or potentially a loss of liver function to convert
560 TMA into TMAO (van den Berg et al., 2023). Reduced *Ruminococcus* abundance correlated with
561 decreased urinary TMAO, reflecting not only microbial shifts but also dietary limitations and potential
562 hepatic enzymatic changes (FMO1 and FMO3) seen in advanced cirrhosis (Organ et al., 2020)
563 (Gatarek and Kaluzna-Czaplinska, 2021; Williams et al., 2010). These data suggest that microbial and
564 dietary disturbances may jointly contribute to the metabolic and immune challenges observed in
565 cirrhosis progression.

566 Further, we noted that patients with cirrhosis exhibited elevated plasma bile acids, especially
567 glycochenodeoxycholic and TCDCA, which correlated with cirrhosis severity. This increase likely
568 stems from impaired hepatic bile acid uptake and reduced conversion to secondary bile acids due to
569 the loss of deconjugating genera like *Lachnospiraceae* and *Ruminococcaceae* genera that were
570 significantly depleted in this cirrhosis cohort (Vital et al., 2019). This impaired conversion could
571 further favour the persistence of *Enterococcus*, as elevated primary bile acids can disrupt the gut
572 microbial ecosystem and inhibit commensal bacteria.

573 Consistent with microbial translocation in cirrhosis, we observed elevated copies of 16S rDNA in the
574 systemic circulation of patients, correlating with cirrhosis severity and reflecting gut barrier
575 dysfunction (Albillos et al., 2022). This microbial translocation, along with elevated faecal calprotectin
576 concentrations, and associated breakdown of gut barrier function and integrity in cirrhosis (Riva et
577 al., 2020), linking with loss of key butyrate-producing microbes like *Ruminococcus* and
578 *Faecalibacterium* genera in DC and ACLF patients (Fagan et al., 2015) (Bach Knudsen et al., 2018).
579 Reduced faecal short-chain fatty acids have been previously reported (Jin et al., 2019; Wang et al.,
580 2023), and a reduced capacity to ferment dietary fibre in cirrhosis patients compared to healthy
581 controls (Jin et al., 2019). *Enterococcus*, which correlated strongly with 16S rDNA copies in the blood,
582 and gut inflammation markers like faecal calprotectin, indicates its likely role in gut inflammation and
583 immune activation in these patients. In cirrhosis, the progressive loss of intestinal barrier integrity
584 allows MAMPs, and viable bacteria, like *Enterococcus*, to translocate into the bloodstream, triggering

585 systemic inflammation and further impairing immune function (Tilg et al., 2022). Indeed, previous
586 work in mice indicates that *E. faecium* triggers colonic cytokine expression, which appears to be strain
587 dependent (Seishima et al., 2019) and related to elevated faecal cytokine levels and other markers
588 of gut barrier dysfunction in DC patients (Riva et al., 2020). Conversely, *Lachnospira* were markedly
589 reduced in cirrhosis patients (Abdugheni et al., 2022), potentially resulting in the loss of the
590 protective role of SCFAs that dampen mucosal immune activation such as through activation and
591 maturation of T regulatory cells (Y et al., 2013). Coupled with impaired immune responses to
592 pathogen-associated TLR signalling, as observed in the CD14+ monocytes of cirrhotic patients, this
593 suggests a vicious cycle of gut perturbations, immune dysfunction, and bacterial translocation that
594 exacerbates systemic inflammation.

595 Interestingly, despite the widespread antibiotic use in the DC and ACLF patients, *Bifidobacterium*
596 persisted in the microbiota of patients with cirrhosis. This genus is typically considered sensitive to
597 antibiotic use (Moubareck et al., 2005), so its resilience here may be due to the frequent use of
598 lactulose, a non-absorbable disaccharide laxative often prescribed to prevent or treat hepatic
599 encephalopathy. Lactulose acts as a prebiotic, providing a substrate that *Bifidobacterium* can
600 metabolise, thereby promoting its growth. Recent studies have shown lactulose can elevate
601 *Bifidobacterium* levels in cirrhosis patients, which inhibited the antibiotic-resistant pathobiont
602 vancomycin-resistant *E. faecium* through potential mechanisms including lowering the luminal pH
603 and via acetate production (Odenwald et al., 2023). Our results add to these recent findings that
604 lactulose supplementation could help support *Bifidobacterium* populations in patients with cirrhosis
605 (Odenwald et al., 2023).

606 From a therapeutic perspective, restoring the gut microbiota toward a healthier balance, or
607 "eubiosis", could mitigate the cycle of immune dysfunction and prevent cirrhosis-related
608 complications (Tranah et al., 2021). Dietary or microbial interventions, such as prebiotics, probiotics,
609 or microbiome-targeted treatments, could offer a promising approach. While faecal microbiota
610 transplantation is currently being trialled (e.g. ClinicalTrials.gov: NCT02862249, NCT06461208,
611 NCT04932577), it carries risks for patients with advanced cirrhosis, where highly personalised or
612 targeted microbiome interventions may be safer (Cibulková et al., 2021) and use of Cefepime to
613 protect anaerobes in gut vs Pip Taz / meropenem. Probiotics or prebiotics aimed at restoring

614 beneficial taxa lost in cirrhosis, such as *Roseburia*, could help inhibit *Enterococcus* overgrowth, and
615 reinforce intestinal barrier integrity, and reduce inflammation. However, these approaches are not
616 available yet clinically or commercially, and significant investment and development is needed to
617 bring such novel, next-generation microbiome-modulating therapies to benefit this patient
618 population. This highlights the urgency for better antimicrobial stewardship and the development of
619 rapid diagnostics that can better target potential pathogens while reducing the use of broad-
620 spectrum antibiotics and deescalating to avoid prolonged courses of exposure.

621 These findings raise the possibility that the overgrowth of *Enterococcus* and loss of commensal
622 microbiota do not merely correlate with disease severity but are also associated with conventional
623 therapies such as the often untargeted use of antibiotics. The absence of a dietary fibre may also
624 contribute to the microbiota disturbances observed, underpinning the crucial role of nutrition in this
625 setting. However, the cross-sectional study design and single time-point sampling limit the ability to
626 infer causality. Longitudinal studies, combined with animal models, could further clarify whether
627 *Enterococcus* contributes to pathological processes in cirrhosis or is an opportunistic response to the
628 disrupted gut environment. Additionally, refined antibiotic strategies, possibly reducing the selective
629 pressure for *Enterococcus*, alongside targeted dietary support to foster beneficial microbes, may
630 represent viable options to improve outcomes for these high-risk patients.

631

632

633 # 4. Methods

634 **Study participants & biological sampling**

635 Patient participants were stratified and phenotyped according to clinically relevant groups based on
636 the severity and time course of their underlying cirrhosis, degree of hepatic decompensation, and
637 presence and extent of hepatic and extra-hepatic organ failure at the time of sampling. These groups
638 were stable cirrhosis (SC; n=15), decompensated cirrhosis (DC; n=55) and acute-on-chronic liver
639 failure (ACLF; n=57), with a separately recruited healthy control cohort (HC; n=40). SC was defined as
640 having Child Pugh A grade(score) of A(5-6). DC was defined by the acute development of 1 or more
641 major complications of cirrhosis, including ascites, HE, variceal haemorrhage, and bacterial infection.
642 ACLF was defined and graded according to the number of organ failures in concordance with criteria
643 reported in the CANONIC study (Arroyo et al., 2015; Moreau et al., 2013). Main exclusion criteria
644 included pregnancy, hepatic or non-hepatic malignancy (HCC within Milan criteria were included),
645 pre-existing immunosuppressive states, replicating HBV/HCV/HIV infection, and known inflammatory
646 bowel disease. Further details are provided in the Supplementary section.

647 Patients were consecutively recruited at King's College Hospital after admission to the ward or when
648 reviewed in the hepatology out-patient clinic, through an observational study and a clinical trial. The
649 observational study was granted approval by the NHS Health Research Authority NRES Committee
650 London Westminster [REC reference: 12/LO/1417] and local sponsor Research and Development
651 department (KCH12-126). Ethical approval for the interventional trial was obtained from NHS Health
652 Research Authority NRES Committee South Central-Oxford C (Bristol) [REC reference: 14/SC/0088]
653 and from the Medicines and Healthcare products Regulatory Agency for Clinical Trial Authorisation
654 [EudraCT number: 2013-004708-20; ClinicalTrials.gov NCT02019784]. The studies were conducted in
655 compliance with the principles of the Declaration of Helsinki (1996), principles of Good Clinical
656 Practice, Research Governance Framework and where relevant, the Medicines for Human Use
657 (Clinical Trial) Regulations. Clinical service users and caregivers were fully consulted and involved in
658 the design of both the study and the trial, and were given opportunities to review and feedback on
659 overall set-up, delivery and practical aspects, including input into development of all participant
660 facing documents. Only baseline pre-intervention data from the clinical trial participants are used in

661 this manuscript. Fully informed consent was obtained from all participants. Some participants eligible
662 for this study were unable to provide informed consent due to cognitive impairment arising from HE
663 and permission from a legal representative was sought.

664 Patient participants, or their legal representative in the case of incapacitation of a potential
665 participant, provided written informed consent within 48 hours of presentation. Patients were
666 managed according to standard evidence-based protocols and guidelines (European Association for
667 the Study of the Liver., 2018). Patient and Public Involvement and Engagement was undertaken with
668 a patient advisory group to determine acceptability of the studies, provided their perspective on
669 study design, informational material, measures to minimise participation burden and agreeing on a
670 dissemination plan of the findings.

671 Demographic, clinical, and biochemical metadata were collected at the time of biological sampling.
672 Standard clinical composite scores used for risk stratification and prognostication included the Child-
673 Pugh score (Pugh et al., 1973), model for end-stage liver disease (MELD) (Kim et al., 2008), United
674 Kingdom model for end-stage liver disease (UKELD) (Asrani and Kim, 2010), and Chronic Liver Failure
675 Consortium-acute decompensation (CLIF-C AD) (Jalan et al., 2015). Healthy controls aged >18 years
676 (n = 40) were recruited to establish reference values for the various assays performed. Exclusion
677 criteria for healthy controls were body mass index <18 or >27; pregnancy or active breastfeeding, a
678 personal history of thrombotic or liver disease; chronic medical conditions requiring regular primary
679 or secondary care review and/or prescribed pharmacotherapies; or current use of anticoagulants,
680 platelet function inhibitors, or oral contraceptives, and no exposure to antibiotics in the previous 6
681 months.

682 **Faecal, urine and blood sample collection and preparation**

683 Plasma samples for bile acid and cytokine profiling were obtained within 24 hours of admission to
684 hospital. Blood was drawn into ethylenediaminetetraacetic acid (EDTA) containing vacuum tubes (BD
685 Vacutainer, Franklin Lakes, NJ, USA). Plasma fractions were collected from these tubes following
686 incubation at room temperature and centrifugation at 2,000 x g for 10 minutes at 4°C. Plasma aliquots
687 were stored immediately at -80°C until further analysis. Whole blood from EDTA tubes was aliquoted
688 into sterile microtubes for and stored immediately at -80°C for bacterial DNA quantification.

689 Urine samples were obtained and centrifugated at 2,000 x g for 10 minutes at 4°C, with the urinary
690 supernatant stored in aliquots for subsequent analysis. Faecal samples for 16S rRNA sequencing and
691 calprotectin quantification were obtained within 48 hours of admission to hospital using non-treated
692 sterile universal tubes. Faecal samples were kept at 4˚C without any preservative and within 6 hours
693 were aliquoted into 1 gram vials for storage at -80˚C. Serum and urine samples were prepared for
694 NMR analyses using standardised protocols (Dona et al., 2014).

695 **Isolation and quality assessment of faecal bacterial DNA**

696 Bacterial DNA was isolated from all faecal samples obtained. This was performed utilising an ISOLATE
697 II Faecal DNA Kit (Bioline, London, UK; BIO-52082). Faecal samples were thawed from -80ºC at room
698 temperature for up to 30 minutes. 150mg of faecal material (crude faecal from each faecal sample)
699 was added directly to a Bashing Beads Lysis Tube (Zymo Research, Orange County, California, USA)
700 and rapidly lysed by bead beating in a vortex, without the use of organic denaturants or proteinases.
701 The DNA was then bound, isolated and purified using spin columns. To optimise the DNA binding
702 step, β-mercaptoethanol (Sigma-Aldrich, Saint Louis, Missouri, USA) was added to eliminate
703 deoxyribonucleases released during cell lysis, by reducing the disulfide bonds within the
704 deoxyribonuclease enzymes. This prevents enzymatic digestion of the DNA during its extraction
705 procedure, increasing the overall yield. The eluted DNA, free of contaminants and enzyme inhibitors,
706 is then used for downstream molecular biology applications including genotyping and sequencing.
707 Extracted DNA concentration and purity were measured using a NanoDrop spectrophotometer
708 (Thermo Fisher Scientific, Australia). Samples with DNA concentrations below the dynamic range of
709 the NanoDrop spectrophotometer were analysed using Qubit High-Sensitivity (HS) dsDNA Assay kit
710 (Life Technologies, Australia).

711 **Faecal 16S rRNA gene amplicon library preparation and sequencing**

712 Amplicons were generated using the method as described previously (Jervis-Bardy et al. 2015). Full
713 details of the library preparation and sequencing protocol are provided in Appendix section 9.3. In
714 brief, barcoded amplicon libraries for the bacterial community analysis on the Illumina MiSeq
715 platform were generated using degenerate primers targeting the V1 and V3 hypervariable regions of
716 the bacterial 16S rRNA gene and Nextera XT index kit (Illumina, Inc., Victoria, Australia).

717 Amplicons were generated using fusion degenerate primers 27 F (5'-
718 TCGTCGGCAGCGTCAGATGTGTATAAGAGACAGAGRGTTTGATCMTGGCTCAG-3') and 519R (5'-
719 GTCTCGTGGGCTCGGAGATGTGTATAAGAGACAGGTNTTACNGCGGCKGCTG-3') with ligated overhang
720 Illumina adapter consensus sequences in italic text. In brief, the initial PCR reactions were performed
721 on a Veriti 96-well Thermal Cycler (Life Technologies, Australia). The PCR reactions were performed
722 in the following programme: initiation enzyme activation at 95°C for 3 min, followed by 25 cycles
723 consisting of denaturation at 95°C for 30 sec, annealing at 55°C for 30 sec and extension at 72°C for
724 30 sec. After 25 cycles, the reaction was completed with a final extension of 7 min at 72°C.

725 The Illumina Nextera XT Index kit (Illumina Inc., San Diego. CA, USA) with dual 8-base indices were
726 used to allow for multiplexing. Two unique indices located on either end of the amplicon were chosen
727 based on the Nextera dual-indexing strategy. To incorporate the indices to the 16S amplicons, PCR
728 reactions were performed on a Veriti 96-well Thermal Cycler (Life Technologies, Australia). Cycling
729 conditions consisted of one cycle of 95°C for 3 min, followed by eight cycles of 95°C for 30 sec, 55°C
730 for 30 sec and 72°C for 30 sec, followed by a final extension cycle of 72°C for 5 min.

731 Prior to library pooling, the barcoded libraries were quantified using the Qubit dsDNA HS Assay Kit
732 (Life Technologies, Carlsbad, CA, USA). Results from this quantification step (amplicon concentration)
733 were used in downstream processing to eliminate contamination. The libraries were sequenced by 2
734 × 300 bp paired-end sequencing on the MiSeq platform using MiSeq v3 Reagent Kit (Illumina) at the
735 Flinders Genomics Facility, Adelaide, Australia. All sequence data generated have been submitted to
736 the Sequence Read Archive (Archive 2014).

737 **16S rRNA amplicon sequencing analysis**

738 The 16S rRNA amplicon sequencing raw reads are deposited in NCBI SRA under project
739 PRJNA1223169. Sequencing reads were analysed using OTU clustering approach via QIIME v1.9.1 as
740 previously described (Kiu et al., 2019). Briefly, raw paired-end reads were firstly merged using PEAR
741 v0.9.6 with -q 30 option (Zhang et al., 2014). Next, quality filtering is performed with
742 split_libraries_fastq.py (QIIME) with -q 29 to retain high-quality reads (Caporaso et al., 2010).
743 Subsequently, chimera removal was performed via chimera identification
744 (identify_chimeric_seqs.py) and chimera sequence removal script (filter_fasta.py). OTU clustering

745 was run via open reference approach (pick_open_reference_otus.py) which does not discard
746 unassigned reads, based on SILVA_132 16S rRNA database optimised for use with QIIME (Quast et
747 al., 2013). BIOM outputs of taxonomic profiles generated from QIIME were then exported using
748 MEGAN v6 (Huson et al., 2016).

749 The sequencing output of 135 samples included one sample containing only 405 sequences and this
750 was discarded from further analysis. The remaining 134 samples contained a mean of 13,905
751 sequences per sample (Standard Deviation 6,497) with a minimum of 2,761 and maximum of 38,637
752 sequences per sample. Rarefaction curves were generated using the rarecurve function in the vegan
753 package (Oksanen, 2017) in R to confirm acceptable levels of sequencing depth. Raw data was
754 normalised using the Deseq2 (Love et al., 2014) package in R using the
755 varianceStabilizingTransformation function.

756 ***Enterococcus* isolation, genomic DNA extraction, Whole Genome Sequencing (WGS) and analysis**

757 Selected faecal samples (~20mg) were subject to serial dilutions in sterile PBS before spread-plating
758 on Slanetz and Bartley agar (Thermo Scientific) for selection of Enterococcus colonies (Slanetz and
759 Bartley, 1957). Subsequently, distinct deep-red coloured colonies, presumably Enterococci, on the
760 agar plates were picked and re-streaked once on fresh Slanetz and Bartley agar after incubation at
761 40°C for 24h. Re-streaked agar plates were then incubated at 40°C for a further 24h to ensure isolate
762 purity prior to overnight culturing in 10ml Brain Heart Infusion media at 40°C to generate sizable
763 bacterial pellets for subsequent genomic DNA extraction. Genomic DNA extraction on the
764 Enterococcus isolates was performed using FastDNA Spin Kit for Soil (MP Biomedicals) as per
765 manufacturer's instructions as described previously (Gooch et al., 2021).

766 Sequencing library was prepared via a modified Illumina Nextera Flex low input tagmentation
767 approach as described previously (Baker et al., 2021; Gooch et al., 2021). Genomic DNA samples were
768 sequenced on Illumina NextSeq 500 with read lengths of 150bp (paired-end).

769 Sequencing reads were quality-filtered and adapter-removed using fastp v0.20.0 with -q 20 option
770 (Chen et al., 2018). Next, short reads were assembled using Unicycler v0.4.9 via primary de novo
771 assembler SPAdes v3.11.1 prior to read polishing via Pilon v1.22. Contigs of length <500 bp were then

772 removed from all draft genome assemblies (Bankevich et al., 2012; Walker et al., 2014; Wick et al.,
773 2017). Taxonomic assignment (Enterococcus faecium) to novel draft genome assemblies were
774 performed using GTDB-Tk v1.5.1 (Chaumeil et al., 2020).

775 A total of 185 E. faecium complete genome assemblies were retrieved from NCBI Genome database
776 (December 2021) for comparison purposes. Together with 5 novel *E. faecium* genomes (n=200), a
777 core gene alignment was generated using Panaroo v1.2.8 with --merge_paralogs option while SNP
778 variants were next extracted by snp-sites v2.3.3 (Page et al., 2016; Tonkin-Hill et al., 2020).
779 Subsequently, a phylogenetic tree was reconstructed via FastTree v2.1 -gtr (-nt) model based on the
780 alignment of core genome SNPs and visualised on iTOL v6 (Letunic and Bork, 2019; Price et al., 2009).

781 Gene search was performed via ABRicate v1.0.1 with --mincov=90 and--minid=90, using databases
782 ARG-ANNOT v6 (AMR genes) and VFDB (Virulence genes) (Gupta et al., 2014; Liu et al., 2019).
783 Nucleotide sequences of bile-salt resistance genes bsh (Accession: AY260046.1) and gltK (Accession:
784 EFF34375.1) were retrieved from GenBank (Benson et al., 2018).

785 **Faecal calprotectin quantification**

786 Faecal calprotectin was measured from frozen faecal samples using a commercially available enzyme-
787 linked immunosorbent assay (Bühlmann Laboratories AG, Schönenbuch, Switzerland) that measures
788 calprotectin in a quantitative manner. This was undertaken in a conventional hospital clinical
789 laboratory (ISO 15189 accredited) with regular interval review of standard operating procedures and
790 equipment calibration. Extraction buffer was added to aliquots of 50mg raw faeces at a
791 weight/volume ratio of 1:50 and homogenised by vortexing for 30 minutes. 2mL of the homogenate
792 was then centrifuged in a microcentrifuge for 5 min at 3000 g. Following centrifugation, the
793 calprotectin ELISA was performed using an automated Grifols Triturus® platform. The ELISA plate is
794 coated with a monoclonal capture antibody highly specific to the calprotectin heterodimeric and
795 polymeric complexes. After incubation, washing, a second incubation with a specific detection
796 antibody, and a further washing step, tetramethylbenzidine (blue colour formation) followed by a
797 stop solution (change to yellow colour) are added by the Triturus. The absorption was determined at
798 an optical density of 450 nm. The linear range of the test was 10-600 µg calprotectin/g faeces with
799 concentration-dependent intra- and inter-assay coefficients of between 2-5% and 4-8%, respectively.

800 **Whole blood 16S ribosomal DNA quantification**

801 The method for quantifying whole blood 16S ribosomal DNA has been previously published in detail
802 (Vergis et al., 2017). Prior to 16S rRNA gene PCR analysis, frozen whole blood samples were thawed
803 to room temperature over a 15-minute period. Mutanolysin (Sigma, St. Louis, Missouri, USA) was
804 added directly to the whole-blood sample; 10µL of 10U/µL enzyme was added for every 200µL of
805 blood being processed, and the sample was incubated for 30 minutes at 37°C.

806 DNA isolation was performed using a total whole blood volume of 200µL per sample. 19µL of
807 10mg/ml lysozyme and 1µL glycogen (Thermo Fisher Scientific; R0561), the latter to aid precipitation,
808 was added to the sample and placed in a water bath at 37°C for 30 minutes. A modified protocol from
809 the QIAmp DNA Blood Mini Kit (Qiagen, Inc., Valencia, CA) was then followed: 200µL of AL buffer was
810 added and the sample vortexed. 20µL of Proteinase K (Thermo Fisher Scientific; EO0491) was then
811 added and then incubated at 56°C for 1 hour in a heat block. After incubation, 200µL of 100% ethanol
812 was added and the resulting lysates were loaded onto the QIAamp DNA Mini kit spin columns.

813 The columns were then centrifuged at 6,000 x g for one minute, and 500µL wash buffer AW1 added,
814 again centrifuged at 6,000 x g for one minute. 500µL wash buffer AW2 was then added, centrifuged
815 at 13,000 x g for three minutes. 50µL of pre-warmed AE elution buffer was added with 5 minutes
816 waiting time, then centrifuged at 13,000 x g for one minute to obtain the DNA extracts. To maximise
817 extraction, the eluate was reapplied to the spin column and centrifuged at 6,000 x g for one minute.
818 PBS and healthy control whole blood PCR were included to quality check for contamination from the
819 process.

820 Real-time polymerase chain reaction (PCR) was used to assess the quantity of bacterial DNA by
821 comparing to known standards. The primers and TaqMan probes were the well-characterized RW01
822 and DG74 primers and TaqMan RDR245 universal probe (synthesized at Applied Biosystems, Foster
823 City, CA) and have been described previously (Jordan and Durso, 2005) with a 380bp 16S rRNA gene
824 target. This target is located in the highly conserved region of 16S bacterial rRNA gene in order to
825 detect the majority of bacterial species found in clinical samples.

826 The forward primer sequence was: 5'-AAC TGG AGG AAG GTG GGG AT3' and the reverse primer
827 sequence was 5'-AGG AGG TGA TCC AAC CGC A-3'. The TaqMan probe sequence was 5'-(6-FAM)-TA

828 CAA GGC CCG GGA ACG TAT TCA CCG-(TAMRA)-3'. Each well contained 5.5µL sterile water (UV
829 irradiated), 1µL RW01 forward primer (10uM), 1µL DG74 reverse primer (10µM), 0.5ul RDR245
830 TaqMan probe (10µM), 10µL of TaqMan Gene Expression Master Mix (Invitrogen; 4369016) and 2µL
831 of sample containing the DNA eluate.

832 A 96 well plate was used and each sample was run in triplicate, and for each plate that was run blank
833 wells were included, a negative control (sterile PBS) and various healthy control samples spiked with
834 a known quantity of E.coli and then serially diluted to generate a standard curve to allow absolute
835 quantification to be calculated. Accordingly, for each PCR run, a standard curve was generated by
836 including a healthy control blood sample which was spiked with known quantities of E.coli (0.4ng,
837 0.04ng, 0.004ng, 0.0004ng, 0.00004ng) using serial 10-fold dilutions and a negative control, also all
838 run in triplicate, and were put through the same DNA extraction process. Any sample displaying a
839 positive signal at or below the level of the negative control was considered negative. Any triplicate
840 group with readings >1 copy cycle apart was considered unreliable and discarded; otherwise, the
841 mean reading was calculated.

842 A StepOnePlus PCR instrument (Invitrogen) was used for real-time PCR, with an initial 2 minutes at
843 50°C and 10-minute denaturation at 95°C, followed by 40 cycles of 15 seconds at 95°C, 30 seconds at
844 60C (annealing) and 1 minute at 72°C (extension). Fluorescence measurements on the PCR
845 instrument were collected during the extension phase of each cycle, and a cycle threshold (C_T) value
846 for each sample and control (including a blank well) was calculated by determining the point at which
847 the fluorescence exceeded the threshold limit, which was set automatically. These values were
848 compared with the *E. coli* standards to obtain a relative quantification of bacterial DNA detected in
849 the whole blood and control samples. Standard curves were generated, and concentrations
850 interpolated in Prism, version 7.0 (GraphPad, La Jolla, CA, USA) The results were extrapolated to
851 picograms of bacterial DNA per millilitre of whole blood.

852 **Plasma cytokine analyses**

853 Plasma cytokines were measured as follows: IL-2, IL-4, IL-6, IL-8, IL-10, IL-12 p70, IL-13, IFN-ɣ, IL1β
854 and TNF-α using an electro-chemiluminescence platform (Meso Scale Discovery (MSD)). Samples
855 were run in duplicate on U-PLEX Proinflam Combo 1 Human™ plates (Cat# K15049K-1, MSD,

856 Gaithersburg, MD). This was conducted according to the manufacturer's protocol. The plate was
857 immediately read on a SECTOR(r) Imager (MSD, Gaithersburg, MD).

858 **Plasma bile acid profiling**

859 Bile acid (BA) profiling was done using an in-house high performance liquid chromatography tandem
860 mass spectrometry (LC-MS/MS) assay modified from published methodology (Tagliacozzi et al.,
861 2003). The method uses an Acentis fusedcore C18 analytical column (15064.6 mm, particle size 2.7
862 mm, Sigma-Aldrich) on a Jasco LC2000 series HPLC system attached to an API 3200 triple quadrupole
863 mass spectrometer (Applied Biosystems, Cheshire, UK). Mobile phases comprised (A) methanol or
864 (B) deionised H2O, each containing 5 mM ammonium acetate (w/v) and 0.012% formic acid (v/v).
865 Negative ion mass spectra of the fractionated BAs were recorded in multiple reaction-monitoring
866 mode. Data were captured using Analyst Software version 1.4.2 (Applied Biosystems) and
867 quantitation carried out by peak area analysis corrected to internal standards (a2,2,4,4,d4-
868 deoxycholic acid for each of the bile acid chemistries; unconjugated, glycine- and taurine-
869 conjugated). The method was linear between 0.1 and 10 mmol/L for all BAs and their conjugates with
870 coefficients of variation (CV %) of 1.5–6.8% at the lower limit of quantitation (0.1 mmol/L). The inter-
871 assay CV was 3.6–8.0%.

872 **Plasma ^{1}H NMR spectroscopy**

873 All plasma samples were prepared according to the previously published papers by Dona et al. and
874 Trovato et al. (Dona et al., 2014; Trovato et al., 2021)[TOO ADD]. ^{1}H NMR spectra were acquired on
875 a Bruker 600 MHz (Avance III) spectrometer, operating at a ^{1}H frequency of 600.16 MHz (14.1 Tesla)
876 at 310K using a 5 mm BBI probe and an automated Sample Jet system (Bruker Biospin, Rheinstetten,
877 Germany). Full explanation of processing is given in the Supplementary section.

878 **Urine ^{1}H NMR spectroscopy**

879 Urinary NMR data were acquired at the Centre for Biomolecular Spectroscopy, King's College London,
880 using a Bruker 600-MHz (AVANCE NEO) NMR spectrometer with a 1H/13C/15N TCI Prodigy (nitrogen-
881 cooled) probe (Bruker, Billerica, USA) as previously described (Bajaj et al., 2019). Pulse-collect NMR
882 data sets were acquired using PURGE water suppression (Le Guennec et al., 2017) and J-resolved

883 NMR sequences. Signal intensities of metabolite regions were obtained using intellibucketing within
884 Wiley KnowItAll® Informatics, Metabolomics Edition v17.0, Wiley Science Solutions, Colorado, USA.
885 NMR spectral regions excluded from the analysis at the outset were 10.0 ppm and 4.5-5.0 ppm
886 (residual water region). Selected intellibucket regions were manually adjusted to incorporate specific
887 metabolite peaks. The binned NMR spectral data outputted from Wiley KnowItAll® Informatics
888 Metabolomics Edition v17.0 were also analysed using MetaboAnalyst v4.0 program (Chong et al.,
889 2018) and exported to the Quadram Institute. Details can be found in the Supplementary section.

890 **Monocyte intracellular cytokine staining**

891 Monocyte intracellular cytokine staining was undertaken using thawed PBMCs from patients with
892 liver disease and at a density of 0.5 millions cells per ml. Cells were either stimulated with TLR2
893 (Pam3CSK4 5ug/ml), Invivogen, France), TLR4 (LPS 100 ng/ml), or TLR9 (CpG 10ug/ml) (Invivogen,
894 France) for 4 hours, or left unstimulated. Monocytes were identified using monoclonal antibodies for
895 surface markers: CD14 PE-Cy7, CD16 APC-H7 (BD Biosciences, UK) and HLA-DR PerCP (ThermoFisher
896 Scientific, UK). Intracellular cytokines were measured using protein transport inhibitor containing
897 monensin, permeabilization/fixation buffer and monoclonal antibodies TNF-α APC and IL-6 PE (BD
898 Biosciences, UK). Percentage positivity in CD14+ monocytes compared with isotype controls (APC
899 mouse IgG1; PE rat IgG2a) were assessed by flow cytometry as previously described (Antoniades et
900 al., 2014). The gating strategy that was employed is shown in Supplementary Figure 1.

901 **Statistical and bioinformatic analyses**

902 For microbiota diversity analysis the number of genera in each sample and the Inverse Simpson
903 diversity was calculated using the specnumber and the diversity functions on genus level taxonomic
904 sequence data in the vegan package (version 2.6-4) in R using raw sequence count data (Oksanen,
905 2017). Differences in alpha-diversity between cirrhosis severity and HC groups was tested with an
906 ANOVA using the aov function in R. Post-hoc pairwise comparisons were determined using the
907 TukeyHSD function in R.

908 To visualise clustering of gut bacterial communities between participants non-metric
909 multidimensional scaling (NMDS) based on a Bray-Curtis distance matrix and using the metaMDS

910 function with k = 3 dimensions contained within the vegan package (version 2.6-4) (Oksanen, 2017).
911 The influence of cirrhosis severity group compared to HC on participant microbiota clustering was
912 tested using a PERMANOVA test using the adonis2 function in the vegan package (version 2.6-4) with
913 a total of 10,000 permutations. Pairwise comparison of clustering of the three cirrhosis severity and
914 HC groups was compared using the pairwiseAdonis function in the pairwiseAdonis package (Martinez
915 Arbizu, 2020).

916 To explore the effect size and significance of associations between clinical metadata variables and
917 beta-diversity of the microbiota within patient samples the envfit function in the vegan package was
918 used to test associations of clinical metadata variables on NMDS ordination calculated using Bray-
919 Curtis dissimilarity after 10,000 permutations. In total, 76 clinical metadata variables were included
920 in the envfit analysis to explore their associations with the gut microbiota composition with three
921 samples excluded during analysis due to missing data (Supplementary File 2). The P-values for
922 combined continuous and factor variables were corrected for multiple comparisons using an FDR
923 adjustment (Benjamini–Hochberg procedure). For visualisation the R2 for the forty significant
924 variables were presented as a bar plot while an arbitrary top ten clinical variables explaining the
925 highest amount of variance (R2) were plotted as an overlay on a NMDS plot of the individual gut
926 microbiota data using the ggplot2 package.

927 Associations between the relative abundance of individual bacterial genera and individual clinical
928 metadata variables were tested using the MaAsLin2 package (Mallick et al., 2021). For genus
929 abundance analysis MaAsLin2 was run with default parameters including multiple testing correction
930 using Benjamini-Hochberg FDR with a significance threshold on adjusted P-values of 0.25 as
931 recommended by the developers. Exceptions to default parameters included an applied minimum
932 prevalence of 0.01 and abundance cut-off of 0.01. Each metadata variable was tested individually.
933 For genus differential abundance analysis cirrhosis severity was included at a Fixed Effect with the
934 HC group as the reference group. For genus differential abundance analysis using antibiotic use, oral
935 food intake, and lactulose use each variable was tested individually. Positive associations were
936 identified antibiotic use, oral food intake, and lactulose and these three variables where combined
937 and tested together as Fixed Effects in a multivariable analysis for the final analysis.

938 Differential analysis of bile acid concentrations was performed using MaAsLin2 with multiple testing
939 correction using Benjamini-Hochberg FDR with a significance threshold on adjusted P-values of 0.25
940 as recommended by the developers. Exceptions to default parameters included no minimum
941 concentration nor abundance cut-off, CLR as the normalisation method and no transformation used.
942 Differential analysis of urinary metabolite and plasma concentrations were analysed using MaAsLin2
943 run with default parameters including multiple testing correction using Benjamini-Hochberg FDR with
944 a significance threshold on adjusted P-values of 0.25 as recommended by the developers. Exceptions
945 to default parameters included no minimum concentration nor abundance cut-off, and no
946 normalisation nor transformation used. The BestNormalize package (version 1.9.1.9000) (Peterson,
947 2021; Peterson and Cavanaugh, 2020) in R was used to optimally normalise each metabolite
948 individually before analysis using the bestnorm function. The method used to transform each variable
949 included in (Supplementary Table 3).

950 For correlation analysis the variables were normalised using the bestnorm function from the
951 bestNormalize package (version 1.9.1.9000). The method used to transform each variable included
952 in (Supplementary Table 4). Pearson correlations were used with statistical significance corrected for
953 multiple testing across genus tested using the False Discovery Rate method.

954

955 # 5. Acknowledgements

956 We are grateful to all the patient participants and healthy volunteers for agreeing to take part in this
957 study, and to the clinical and liver research teams at King's College Hospital for facilitating
958 recruitment, collecting metadata and biological sample collection. We are grateful to Dr Mark
959 McPhail for methodological guidance and expertise on plasma NMR data generation. We thank the
960 King's College Hospital Charity and a generous donation from a Liver Service User, and the
961 Foundation for Liver Research for funding. Sequencing analysis was supported in part by the NBI
962 Research Computing through the provision of a High Performance Computing. The authors thank the
963 Centre for Biomolecular Spectroscopy funded by the Wellcome Trust and British Heart Foundation
964 (ref. 202767/Z/16/Z and IG/16/2/32273).

6. References

Abdugheni, R., Wang, W.-Z., Wang, Y.-J., Du, M.-X., Liu, F.-L., Zhou, N., Jiang, C.-Y., Wang, C.-Y., Wu, L., Ma, J., Liu, C., Liu, S.-J., 2022. Metabolite profiling of human-originated Lachnospiraceae at the strain level. iMeta 1, e58. https://doi.org/10.1002/imt2.58

Acharya, C., Bajaj, J.S., 2019. Altered Microbiome in Patients With Cirrhosis and Complications. Clin Gastroenterol Hepatol 17, 307–321. https://doi.org/10.1016/j.cgh.2018.08.008

Adak, A., Khan, M.R., 2019. An insight into gut microbiota and its functionalities. Cell Mol Life Sci 76, 473–493. https://doi.org/10.1007/s00018-018-2943-4

Albillos, A., de Gottardi, A., Rescigno, M., 2020. The gut-liver axis in liver disease: Pathophysiological basis for therapy. J Hepatol 72, 558–577. https://doi.org/10.1016/j.jhep.2019.10.003

Albillos, A., Martin-Mateos, R., Van der Merwe, S., Wiest, R., Jalan, R., Álvarez-Mon, M., 2022. Cirrhosis-associated immune dysfunction. Nat Rev Gastroenterol Hepatol 19, 112–134. https://doi.org/10.1038/s41575-021-00520-7

Alexopoulou, A., Agiasotelli, D., Vasilieva, L.E., Dourakis, S.P., 2017. Bacterial translocation markers in liver cirrhosis. Ann Gastroenterol 30, 486–497. https://doi.org/10.20524/aog.2017.0178

Antoniades, C.G., Khamri, W., Abeles, R.D., Taams, L.S., Triantafyllou, E., Possamai, L.A., Bernsmeier, C., Mitry, R.R., O'Brien, A., Gilroy, D., Goldin, R., Heneghan, M., Heaton, N., Jassem, W., Bernal, W., Vergani, D., Ma, Y., Quaglia, A., Wendon, J., Thursz, M., 2014. Secretory leukocyte protease inhibitor: a pivotal mediator of anti-inflammatory responses in acetaminophen-induced acute liver failure. Hepatology 59, 1564–1576. https://doi.org/10.1002/hep.26933

Arroyo, V., Moreau, R., Jalan, R., Ginès, P., EASL-CLIF Consortium CANONIC Study, 2015. Acute-on-chronic liver failure: A new syndrome that will re-classify cirrhosis. J Hepatol 62, S131-143. https://doi.org/10.1016/j.jhep.2014.11.045

Asrani, S.K., Kim, W.R., 2010. Organ allocation for chronic liver disease: model for end-stage liver disease and beyond. Curr Opin Gastroenterol 26, 209–213. https://doi.org/10.1097/MOG.0b013e32833867d8

Bach Knudsen, K.E., Lærke, H.N., Hedemann, M.S., Nielsen, T.S., Ingerslev, A.K., Gundelund Nielsen, D.S., Theil, P.K., Purup, S., Hald, S., Schioldan, A.G., Marco, M.L., Gregersen, S., Hermansen, K., 2018. Impact of Diet-Modulated Butyrate Production on Intestinal Barrier Function and Inflammation. Nutrients 10, 1499. https://doi.org/10.3390/nu10101499

Bajaj, J.S., Heuman, D.M., Hylemon, P.B., Sanyal, A.J., White, M.B., Monteith, P., Noble, N.A., Unser, A.B., Daita, K., Fisher, A.R., Sikaroodi, M., Gillevet, P.M., 2014. Altered profile of human gut microbiome is associated with cirrhosis and its complications. Journal of Hepatology 60, 940–947. https://doi.org/10.1016/j.jhep.2013.12.019

Bajaj, J.S., Reddy, K.R., Tandon, P., Garcia-Tsao, G., Kamath, P.S., O'Leary, J.G., Wong, F., Lai, J., Vargas, H., Thuluvath, P.J., Subramanian, R.M., Pena-Rodriguez, M., Sikaroodi, M., Thacker, L.R., Gillevet, P.M., 2022. Association of serum metabolites and gut microbiota at hospital admission with nosocomial infection development in patients with cirrhosis. Liver Transpl 28, 1831–1840. https://doi.org/10.1002/lt.26552

Bajaj, J.S., Ridlon, J.M., Hylemon, P.B., Thacker, L.R., Heuman, D.M., Smith, S., Sikaroodi, M., Gillevet, P.M., 2012. Linkage of gut microbiome with cognition in hepatic encephalopathy. Am J Physiol Gastrointest Liver Physiol 302, G168-175. https://doi.org/10.1152/ajpgi.00190.2011

1010 Bajaj, J.S., Salzman, N., Acharya, C., Takei, H., Kakiyama, G., Fagan, A., White, M.B., Gavis, E.A., Holtz,
1011 M.L., Hayward, M., Nittono, H., Hylemon, P.B., Cox, I.J., Williams, R., Taylor-Robinson, S.D.,
1012 Sterling, R.K., Matherly, S.C., Fuchs, M., Lee, H., Puri, P., Stravitz, R.T., Sanyal, A.J., Ajayi, L., Le
1013 Guennec, A., Atkinson, R.A., Siddiqui, M.S., Luketic, V., Pandak, W.M., Sikaroodi, M., Gillevet,
1014 P.M., 2019. Microbial functional change is linked with clinical outcomes after capsular fecal
1015 transplant in cirrhosis. JCI Insight 4, e133410, 133410.
1016 https://doi.org/10.1172/jci.insight.133410
1017 Baker, D.J., Aydin, A., Le-Viet, T., Kay, G.L., Rudder, S., de Oliveira Martins, L., Tedim, A.P., Kolyva, A.,
1018 Diaz, M., Alikhan, N.-F., Meadows, L., Bell, A., Gutierrez, A.V., Trotter, A.J., Thomson, N.M.,
1019 Gilroy, R., Griffith, L., Adriaenssens, E.M., Stanley, R., Charles, I.G., Elumogo, N., Wain, J.,
1020 Prakash, R., Meader, E., Mather, A.E., Webber, M.A., Dervisevic, S., Page, A.J., O'Grady, J.,
1021 2021. CoronaHiT: high-throughput sequencing of SARS-CoV-2 genomes. Genome Medicine
1022 13, 21. https://doi.org/10.1186/s13073-021-00839-5
1023 Bankevich, A., Nurk, S., Antipov, D., Gurevich, A.A., Dvorkin, M., Kulikov, A.S., Lesin, V.M., Nikolenko,
1024 S.I., Pham, S., Prjibelski, A.D., Pyshkin, A.V., Sirotkin, A.V., Vyahhi, N., Tesler, G., Alekseyev,
1025 M.A., Pevzner, P.A., 2012. SPAdes: a new genome assembly algorithm and its applications to
1026 single-cell sequencing. J Comput Biol 19, 455–477. https://doi.org/10.1089/cmb.2012.0021
1027 Benson, D.A., Cavanaugh, M., Clark, K., Karsch-Mizrachi, I., Ostell, J., Pruitt, K.D., Sayers, E.W., 2018.
1028 GenBank. Nucleic Acids Research 46, D41–D47. https://doi.org/10.1093/nar/gkx1094
1029 Caballero-Flores, G., Pickard, J.M., Núñez, G., 2023. Microbiota-mediated colonization resistance:
1030 mechanisms and regulation. Nat Rev Microbiol 21, 347–360. https://doi.org/10.1038/s41579-
1031 022-00833-7
1032 Caporaso, J.G., Kuczynski, J., Stombaugh, J., Bittinger, K., Bushman, F.D., Costello, E.K., Fierer, N.,
1033 Peña, A.G., Goodrich, J.K., Gordon, J.I., Huttley, G.A., Kelley, S.T., Knights, D., Koenig, J.E., Ley,
1034 R.E., Lozupone, C.A., McDonald, D., Muegge, B.D., Pirrung, M., Reeder, J., Sevinsky, J.R.,
1035 Turnbaugh, P.J., Walters, W.A., Widmann, J., Yatsunenko, T., Zaneveld, J., Knight, R., 2010.
1036 QIIME allows analysis of high-throughput community sequencing data. Nat Methods 7, 335–
1037 336. https://doi.org/10.1038/nmeth.f.303
1038 Chaumeil, P.-A., Mussig, A.J., Hugenholtz, P., Parks, D.H., 2020. GTDB-Tk: a toolkit to classify genomes
1039 with the Genome Taxonomy Database. Bioinformatics 36, 1925–1927.
1040 https://doi.org/10.1093/bioinformatics/btz848
1041 Chen, S., Zhou, Y., Chen, Y., Gu, J., 2018. fastp: an ultra-fast all-in-one FASTQ preprocessor.
1042 Bioinformatics 34, i884–i890. https://doi.org/10.1093/bioinformatics/bty560
1043 Chong, J., Soufan, O., Li, C., Caraus, I., Li, S., Bourque, G., Wishart, D.S., Xia, J., 2018. MetaboAnalyst
1044 4.0: towards more transparent and integrative metabolomics analysis. Nucleic acids research
1045 46. https://doi.org/10.1093/nar/gky310
1046 Cibulková, I., Řehořová, V., Hajer, J., Duška, F., 2021. Fecal Microbial Transplantation in Critically Ill
1047 Patients—Structured Review and Perspectives. Biomolecules 11, 1459.
1048 https://doi.org/10.3390/biom11101459
1049 Da Silva, H.E., Teterina, A., Comelli, E.M., Taibi, A., Arendt, B.M., Fischer, S.E., Lou, W., Allard, J.P.,
1050 2018. Nonalcoholic fatty liver disease is associated with dysbiosis independent of body mass
1051 index and insulin resistance. Sci Rep 8, 1466. https://doi.org/10.1038/s41598-018-19753-9
1052 D'Amico, G., Bernardi, M., Angeli, P., 2022. Towards a new definition of decompensated cirrhosis.
1053 Journal of Hepatology 76, 202–207. https://doi.org/10.1016/j.jhep.2021.06.018

1054 Dona, A.C., Jiménez, B., Schäfer, H., Humpfer, E., Spraul, M., Lewis, M.R., Pearce, J.T.M., Holmes, E.,
1055 Lindon, J.C., Nicholson, J.K., 2014. Precision high-throughput proton NMR spectroscopy of
1056 human urine, serum, and plasma for large-scale metabolic phenotyping. Anal Chem 86, 9887–
1057 9894. https://doi.org/10.1021/ac5025039
1058 Dubinkina, V.B., Tyakht, A.V., Odintsova, V.Y., Yarygin, K.S., Kovarsky, B.A., Pavlenko, A.V., Ischenko,
1059 D.S., Popenko, A.S., Alexeev, D.G., Taraskina, A.Y., Nasyrova, R.F., Krupitsky, E.M., Shalikiani,
1060 N.V., Bakulin, I.G., Shcherbakov, P.L., Skorodumova, L.O., Larin, A.K., Kostryukova, E.S.,
1061 Abdulkhakov, R.A., Abdulkhakov, S.R., Malanin, S.Y., Ismagilova, R.K., Grigoryeva, T.V., Ilina,
1062 E.N., Govorun, V.M., 2017. Links of gut microbiota composition with alcohol dependence
1063 syndrome and alcoholic liver disease. Microbiome 5, 141. https://doi.org/10.1186/s40168-
1064 017-0359-2
1065 European Association for the Study of the Liver., 2018. EASL Clinical Practice Guidelines for the
1066 management of patients with decompensated cirrhosis. J Hepatol 69, 406–460.
1067 https://doi.org/10.1016/j.jhep.2018.03.024
1068 Fagan, K.J., Rogers, G.B., Melino, M., Arthur, D.M., Costello, M.-E., Morrison, M., Powell, E.E., Irvine,
1069 K.M., 2015. Ascites Bacterial Burden and Immune Cell Profile Are Associated with Poor Clinical
1070 Outcomes in the Absence of Overt Infection. PLoS One 10, e0120642.
1071 https://doi.org/10.1371/journal.pone.0120642
1072 Flint, H.J., Scott, K.P., Duncan, S.H., Louis, P., Forano, E., 2012. Microbial degradation of complex
1073 carbohydrates in the gut. Gut Microbes 3, 289–306. https://doi.org/10.4161/gmic.19897
1074 Garrett, W.S., 2020. Enterococcus in Graft-versus-Host Disease. N Engl J Med 382, 1064–1066.
1075 https://doi.org/10.1056/NEJMcibr1915978
1076 Gatarek, P., Kaluzna-Czaplinska, J., 2021. Trimethylamine N-oxide (TMAO) in human health. EXCLI J
1077 20, 301–319. https://doi.org/10.17179/excli2020-3239
1078 Ghosh, S., Whitley, C.S., Haribabu, B., Jala, V.R., 2021. Regulation of Intestinal Barrier Function by
1079 Microbial Metabolites. Cellular and Molecular Gastroenterology and Hepatology 11, 1463–
1080 1482. https://doi.org/10.1016/j.jcmgh.2021.02.007
1081 Gooch, H.C.C., Kiu, R., Rudder, S., Baker, D.J., Hall, L.J., Maxwell, A., 2021. Enterococcus innesii sp.
1082 nov., isolated from the wax moth Galleria mellonella. Int J Syst Evol Microbiol 71, 005168.
1083 https://doi.org/10.1099/ijsem.0.005168
1084 Gupta, S.K., Padmanabhan, B.R., Diene, S.M., Lopez-Rojas, R., Kempf, M., Landraud, L., Rolain, J.-M.,
1085 2014. ARG-ANNOT, a New Bioinformatic Tool To Discover Antibiotic Resistance Genes in
1086 Bacterial Genomes. Antimicrob Agents Chemother 58, 212–220.
1087 https://doi.org/10.1128/AAC.01310-13
1088 Hendrickx, A.P.A., van Luit-Asbroek, M., Schapendonk, C.M.E., van Wamel, W.J.B., Braat, J.C.,
1089 Wijnands, L.M., Bonten, M.J.M., Willems, R.J.L., 2009. SgrA, a nidogen-binding LPXTG surface
1090 adhesin implicated in biofilm formation, and EcbA, a collagen binding MSCRAMM, are two
1091 novel adhesins of hospital-acquired Enterococcus faecium. Infect Immun 77, 5097–5106.
1092 https://doi.org/10.1128/IAI.00275-09
1093 Hernaez, R., Solà, E., Moreau, R., Ginès, P., 2017. Acute-on-chronic liver failure: an update. Gut 66,
1094 541–553. https://doi.org/10.1136/gutjnl-2016-312670
1095 Horvatits, T., Drolz, A., Roedl, K., Rutter, K., Ferlitsch, A., Fauler, G., Trauner, M., Fuhrmann, V., 2017.
1096 Serum bile acids as marker for acute decompensation and acute-on-chronic liver failure in
1097 patients with non-cholestatic cirrhosis. Liver Int 37, 224–231.
1098 https://doi.org/10.1111/liv.13201

1099 Hsu, C.L., Schnabl, B., 2023. The gut–liver axis and gut microbiota in health and liver disease. Nat Rev
1100 Microbiol 21, 719–733. https://doi.org/10.1038/s41579-023-00904-3
1101 Huang, D.Q., Terrault, N.A., Tacke, F., Gluud, L.L., Arrese, M., Bugianesi, E., Loomba, R., 2023. Global
1102 epidemiology of cirrhosis — aetiology, trends and predictions. Nat Rev Gastroenterol Hepatol
1103 20, 388–398. https://doi.org/10.1038/s41575-023-00759-2
1104 Hufnagel, M., Liese, C., Loescher, C., Kunze, M., Proempeler, H., Berner, R., Krueger, M., 2007.
1105 Enterococcal colonization of infants in a neonatal intensive care unit: associated predictors,
1106 risk factors and seasonal patterns. BMC Infect Dis 7, 107. https://doi.org/10.1186/1471-2334-
1107 7-107
1108 Huson, D.H., Beier, S., Flade, I., Górska, A., El-Hadidi, M., Mitra, S., Ruscheweyh, H.-J., Tappu, R., 2016.
1109 MEGAN Community Edition - Interactive Exploration and Analysis of Large-Scale Microbiome
1110 Sequencing Data. PLOS Computational Biology 12, e1004957.
1111 https://doi.org/10.1371/journal.pcbi.1004957
1112 Jalan, R., Pavesi, M., Saliba, F., Amorós, A., Fernandez, J., Holland-Fischer, P., Sawhney, R., Mookerjee,
1113 R., Caraceni, P., Moreau, R., Ginès, P., Durand, F., Angeli, P., Alessandria, C., Laleman, W.,
1114 Trebicka, J., Samuel, D., Zeuzem, S., Gustot, T., Gerbes, A.L., Wendon, J., Bernardi, M., Arroyo,
1115 V., CANONIC Study Investigators; EASL-CLIF Consortium, 2015. The CLIF Consortium Acute
1116 Decompensation score (CLIF-C ADs) for prognosis of hospitalised cirrhotic patients without
1117 acute-on-chronic liver failure. J Hepatol 62, 831–840.
1118 https://doi.org/10.1016/j.jhep.2014.11.012
1119 Jin, M., Kalainy, S., Baskota, N., Chiang, D., Deehan, E.C., McDougall, C., Tandon, P., Martínez, I.,
1120 Cervera, C., Walter, J., Abraldes, J.G., 2019. Faecal microbiota from patients with cirrhosis has
1121 a low capacity to ferment non-digestible carbohydrates into short-chain fatty acids. Liver Int
1122 39, 1437–1447. https://doi.org/10.1111/liv.14106
1123 Jordan, J.A., Durso, M.B., 2005. Real-time polymerase chain reaction for detecting bacterial DNA
1124 directly from blood of neonates being evaluated for sepsis. J Mol Diagn 7, 575–581.
1125 https://doi.org/10.1016/S1525-1578(10)60590-9
1126 Kakiyama, G., Muto, A., Takei, H., Nittono, H., Murai, T., Kurosawa, T., Hofmann, A.F., Pandak, W.M.,
1127 Bajaj, J.S., 2014. A simple and accurate HPLC method for fecal bile acid profile in healthy and
1128 cirrhotic subjects: validation by GC-MS and LC-MS. J Lipid Res 55, 978–990.
1129 https://doi.org/10.1194/jlr.D047506
1130 Kakiyama, G., Pandak, W.M., Gillevet, P.M., Hylemon, P.B., Heuman, D.M., Daita, K., Takei, H., Muto,
1131 A., Nittono, H., Ridlon, J.M., White, M.B., Noble, N.A., Monteith, P., Fuchs, M., Thacker, L.R.,
1132 Sikaroodi, M., Bajaj, J.S., 2013. Modulation of the fecal bile acid profile by gut microbiota in
1133 cirrhosis. J Hepatol 58, 949–955. https://doi.org/10.1016/j.jhep.2013.01.003
1134 Katoonizadeh, A., Laleman, W., Verslype, C., Wilmer, A., Maleux, G., Roskams, T., Nevens, F., 2010.
1135 Early features of acute-on-chronic alcoholic liver failure: a prospective cohort study. Gut 59,
1136 1561–1569. https://doi.org/10.1136/gut.2009.189639
1137 Kim, W.R., Biggins, S.W., Kremers, W.K., Wiesner, R.H., Kamath, P.S., Benson, J.T., Edwards, E.,
1138 Therneau, T.M., 2008. Hyponatremia and mortality among patients on the liver-transplant
1139 waiting list. N Engl J Med 359, 1018–1026. https://doi.org/10.1056/NEJMoa0801209
1140 Kiu, R., Brown, J., Bedwell, H., Leclaire, C., Caim, S., Pickard, D., Dougan, G., Dixon, R.A., Hall, L.J.,
1141 2019. Genomic analysis on broiler-associated Clostridium perfringens strains and exploratory
1142 caecal microbiome investigation reveals key factors linked to poultry necrotic enteritis.
1143 Animal Microbiome 1, 12. https://doi.org/10.1186/s42523-019-0015-1

1144 Le Guennec, A., Tayyari, F., Edison, A.S., 2017. Alternatives to Nuclear Overhauser Enhancement
1145 Spectroscopy Presat and Carr-Purcell-Meiboom-Gill Presat for NMR-Based Metabolomics.
1146 Anal Chem 89, 8582–8588. https://doi.org/10.1021/acs.analchem.7b02354
1147 Lee, S., Arefaine, B., Begum, N., Stamouli, M., Witherden, E., Mohamad, M., Harzandi, A., Zamalloa,
1148 A., Cai, H., Williams, R., Curtis, M., Edwards, L.A., Chokshi, S., Mardinoglu, A., Proctor, G.,
1149 Moyes, D., McPhail, M.J., Shawcross, D.L., Uhlen, M., Shoaie, S., Patel, V.C., 2024a. Oral-gut
1150 microbiome interactions in advanced cirrhosis: characterisation of pathogenic enterotypes
1151 and salivatypes, virulence factors and antimicrobial. J Hepatol S0168-8278(24)02635–7.
1152 https://doi.org/10.1016/j.jhep.2024.09.046
1153 Lee, S., Arefaine, B., Begum, N., Stamouli, M., Witherden, E., Mohamad, M., Harzandi, A., Zamalloa,
1154 A., Cai, H., Williams, R., Curtis, M.A., Edwards, L.A., Chokshi, S., Mardinoglu, A., Proctor, G.,
1155 Moyes, D.L., McPhail, M.J., Shawcross, D.L., Uhlen, M., Shoaie, S., Patel, V.C., 2024b. Oral-gut
1156 microbiome interactions in advanced cirrhosis: characterisation of pathogenic enterotypes
1157 and salivatypes, virulence factors and antimicrobial resistance. Journal of Hepatology 0.
1158 https://doi.org/10.1016/j.jhep.2024.09.046
1159 Lees, H.J., Swann, J.R., Wilson, I.D., Nicholson, J.K., Holmes, E., 2013. Hippurate: the natural history
1160 of a mammalian-microbial cometabolite. J Proteome Res 12, 1527–1546.
1161 https://doi.org/10.1021/pr300900b
1162 Letunic, I., Bork, P., 2019. Interactive Tree Of Life (iTOL) v4: recent updates and new developments.
1163 Nucleic Acids Research 47, W256–W259. https://doi.org/10.1093/nar/gkz239
1164 Liu, B., Zheng, D., Jin, Q., Chen, L., Yang, J., 2019. VFDB 2019: a comparative pathogenomic platform
1165 with an interactive web interface. Nucleic Acids Research 47, D687–D692.
1166 https://doi.org/10.1093/nar/gky1080
1167 Love, M.I., Huber, W., Anders, S., 2014. Moderated estimation of fold change and dispersion for RNA-
1168 seq data with DESeq2. Genome Biol 15, 550. https://doi.org/10.1186/s13059-014-0550-8
1169 Mallick, H., Rahnavard, A., McIver, L.J., Ma, S., Zhang, Y., Nguyen, L.H., Tickle, T.L., Weingart, G., Ren,
1170 B., Schwager, E.H., Chatterjee, S., Thompson, K.N., Wilkinson, J.E., Subramanian, A., Lu, Y.,
1171 Waldron, L., Paulson, J.N., Franzosa, E.A., Bravo, H.C., Huttenhower, C., 2021. Multivariable
1172 association discovery in population-scale meta-omics studies. PLOS Computational Biology
1173 17, e1009442. https://doi.org/10.1371/journal.pcbi.1009442
1174 Martinez Arbizu, P., 2020. pairwiseAdonis: Pairwise multilevel comparison using adonis.
1175 Moreau, R., Jalan, R., Gines, P., Pavesi, M., Angeli, P., Cordoba, J., Durand, F., Gustot, T., Saliba, F.,
1176 Domenicali, M., Gerbes, A., Wendon, J., Alessandria, C., Laleman, W., Zeuzem, S., Trebicka, J.,
1177 Bernardi, M., Arroyo, V., CANONIC Study Investigators of the EASL–CLIF Consortium, 2013.
1178 Acute-on-chronic liver failure is a distinct syndrome that develops in patients with acute
1179 decompensation of cirrhosis. Gastroenterology 144, 1426–1437, 1437.e1–9.
1180 https://doi.org/10.1053/j.gastro.2013.02.042
1181 Moubareck, C., Gavini, F., Vaugien, L., Butel, M.J., Doucet-Populaire, F., 2005. Antimicrobial
1182 susceptibility of bifidobacteria. J Antimicrob Chemother 55, 38–44.
1183 https://doi.org/10.1093/jac/dkh495
1184 Mouzaki, M., Wang, A.Y., Bandsma, R., Comelli, E.M., Arendt, B.M., Zhang, L., Fung, S., Fischer, S.E.,
1185 McGilvray, I.G., Allard, J.P., 2016. Bile Acids and Dysbiosis in Non-Alcoholic Fatty Liver Disease.
1186 PLoS One 11, e0151829. https://doi.org/10.1371/journal.pone.0151829
1187 Nallapareddy, S.R., Singh, K.V., Okhuysen, P.C., Murray, B.E., 2008. A functional collagen adhesin
1188 gene, acm, in clinical isolates of Enterococcus faecium correlates with the recent success of

1189 this emerging nosocomial pathogen. Infect Immun 76, 4110–4119.
1190 https://doi.org/10.1128/IAI.00375-08
1191 Odenwald, M.A., Lin, H., Lehmann, C., Dylla, N.P., Cole, C.G., Mostad, J.D., Pappas, T.E., Ramaswamy,
1192 R., Moran, A., Hutchison, A.L., Stutz, M.R., Dela Cruz, M., Adler, E., Boissiere, J., Khalid, M.,
1193 Cantoral, J., Haro, F., Oliveira, R.A., Waligurski, E., Cotter, T.G., Light, S.H., Beavis, K.G.,
1194 Sundararajan, A., Sidebottom, A.M., Reddy, K.G., Paul, S., Pillai, A., Te, H.S., Rinella, M.E.,
1195 Charlton, M.R., Pamer, E.G., Aronsohn, A.I., 2023. Bifidobacteria metabolize lactulose to
1196 optimize gut metabolites and prevent systemic infection in patients with liver disease. Nat
1197 Microbiol 1–17. https://doi.org/10.1038/s41564-023-01493-w
1198 Oksanen, F., 2017. Vegan: Community Ecology Package.
1199 Organ, C.L., Li, Z., Sharp, T.E., Polhemus, D.J., Gupta, N., Goodchild, T.T., Tang, W.H.W., Hazen, S.L.,
1200 Lefer, D.J., 2020. Nonlethal Inhibition of Gut Microbial Trimethylamine N-oxide Production
1201 Improves Cardiac Function and Remodeling in a Murine Model of Heart Failure. Journal of the
1202 American Heart Association 9, e016223. https://doi.org/10.1161/JAHA.119.016223
1203 Page, A.J., Taylor, B., Delaney, A.J., Soares, J., Seemann, T., Keane, J.A., Harris, S.R., 2016. SNP-sites:
1204 rapid efficient extraction of SNPs from multi-FASTA alignments. Microb Genom 2, e000056.
1205 https://doi.org/10.1099/mgen.0.000056
1206 Pallister, T., Jackson, M.A., Martin, T.C., Zierer, J., Jennings, A., Mohney, R.P., MacGregor, A., Steves,
1207 C.J., Cassidy, A., Spector, T.D., Menni, C., 2017. Hippurate as a metabolomic marker of gut
1208 microbiome diversity: Modulation by diet and relationship to metabolic syndrome. Sci Rep 7,
1209 13670. https://doi.org/10.1038/s41598-017-13722-4
1210 Peterson, R.A., 2021. Finding Optimal Normalizing Transformations via bestNormalize. The R Journal
1211 13, 310–329.
1212 Peterson, R.A., Cavanaugh, J.E., 2020. Ordered quantile normalization: a semiparametric
1213 transformation built for the cross-validation era. Journal of Applied Statistics 47, 2312–2327.
1214 https://doi.org/10.1080/02664763.2019.1630372
1215 Piano, S., Singh, V., Caraceni, P., Maiwall, R., Alessandria, C., Fernandez, J., Soares, E.C., Kim, D.J., Kim,
1216 S.E., Marino, M., Vorobioff, J., Barea, R. de C.R., Merli, M., Elkrief, L., Vargas, V., Krag, A., Singh,
1217 S.P., Lesmana, L.A., Toledo, C., Marciano, S., Verhelst, X., Wong, F., Intagliata, N., Rabinowich,
1218 L., Colombato, L., Kim, S.G., Gerbes, A., Durand, F., Roblero, J.P., Bhamidimarri, K.R., Boyer,
1219 T.D., Maevskaya, M., Fassio, E., Kim, H.S., Hwang, J.S., Gines, P., Gadano, A., Sarin, S.K., Angeli,
1220 P., International Club of Ascites Global Study Group, 2019. Epidemiology and Effects of
1221 Bacterial Infections in Patients With Cirrhosis Worldwide. Gastroenterology 156, 1368-
1222 1380.e10. https://doi.org/10.1053/j.gastro.2018.12.005
1223 Price, M.N., Dehal, P.S., Arkin, A.P., 2009. FastTree: Computing Large Minimum Evolution Trees with
1224 Profiles instead of a Distance Matrix. Molecular Biology and Evolution 26, 1641–1650.
1225 https://doi.org/10.1093/molbev/msp077
1226 Pugh, R.N., Murray-Lyon, I.M., Dawson, J.L., Pietroni, M.C., Williams, R., 1973. Transection of the
1227 oesophagus for bleeding oesophageal varices. Br J Surg 60, 646–649.
1228 https://doi.org/10.1002/bjs.1800600817
1229 Quast, C., Pruesse, E., Yilmaz, P., Gerken, J., Schweer, T., Yarza, P., Peplies, J., Glöckner, F.O., 2013.
1230 The SILVA ribosomal RNA gene database project: improved data processing and web-based
1231 tools. Nucleic Acids Research 41, D590–D596. https://doi.org/10.1093/nar/gks1219

1232 Ridlon, J.M., Alves, J.M., Hylemon, P.B., Bajaj, J.S., 2013. Cirrhosis, bile acids and gut microbiota:
1233 unraveling a complex relationship. Gut Microbes 4, 382–387.
1234 https://doi.org/10.4161/gmic.25723
1235 Riva, A., Gray, E.H., Azarian, S., Zamalloa, A., McPhail, M.J.W., Vincent, R.P., Williams, R., Chokshi, S.,
1236 Patel, V.C., Edwards, L.A., 2020. Faecal cytokine profiling as a marker of intestinal
1237 inflammation in acutely decompensated cirrhosis. JHEP Rep 2, 100151.
1238 https://doi.org/10.1016/j.jhepr.2020.100151
1239 Seishima, J., Iida, N., Kitamura, K., Yutani, M., Wang, Z., Seki, A., Yamashita, Taro, Sakai, Y., Honda,
1240 M., Yamashita, Tatsuya, Kagaya, T., Shirota, Y., Fujinaga, Y., Mizukoshi, E., Kaneko, S., 2019.
1241 Gut-derived Enterococcus faecium from ulcerative colitis patients promotes colitis in a
1242 genetically susceptible mouse host. Genome Biol 20, 252. https://doi.org/10.1186/s13059-
1243 019-1879-9
1244 Shah, N.J., Mousa, O.Y., Syed, K., John, S., 2024. Acute on Chronic Liver Failure, in: StatPearls.
1245 StatPearls Publishing, Treasure Island (FL).
1246 Slanetz, L.W., Bartley, C.H., 1957. NUMBERS OF ENTEROCOCCI IN WATER, SEWAGE, AND FECES
1247 DETERMINED BY THE MEMBRANE FILTER TECHNIQUE WITH AN IMPROVED MEDIUM1. J
1248 Bacteriol 74, 591–595.
1249 Solé, C., Guilly, S., Da Silva, K., Llopis, M., Le-Chatelier, E., Huelin, P., Carol, M., Moreira, R., Fabrellas,
1250 N., De Prada, G., Napoleone, L., Graupera, I., Pose, E., Juanola, A., Borruel, N., Berland, M.,
1251 Toapanta, D., Casellas, F., Guarner, F., Doré, J., Solà, E., Ehrlich, S.D., Ginès, P., 2021.
1252 Alterations in Gut Microbiome in Cirrhosis as Assessed by Quantitative Metagenomics:
1253 Relationship With Acute-on-Chronic Liver Failure and Prognosis. Gastroenterology 160, 206-
1254 218.e13. https://doi.org/10.1053/j.gastro.2020.08.054
1255 Tagliacozzi, D., Mozzi, A.F., Casetta, B., Bertucci, P., Bernardini, S., Di Ilio, C., Urbani, A., Federici, G.,
1256 2003. Quantitative analysis of bile acids in human plasma by liquid chromatography-
1257 electrospray tandem mass spectrometry: a simple and rapid one-step method. Clin Chem Lab
1258 Med 41, 1633–1641. https://doi.org/10.1515/CCLM.2003.247
1259 Tilg, H., Adolph, T.E., Trauner, M., 2022. Gut-liver axis: Pathophysiological concepts and clinical
1260 implications. Cell Metab 34, 1700–1718. https://doi.org/10.1016/j.cmet.2022.09.017
1261 Toledo, C., Salmerón, J.M., Rimola, A., Navasa, M., Arroyo, V., Llach, J., Ginès, A., Ginès, P., Rodés, J.,
1262 1993. Spontaneous bacterial peritonitis in cirrhosis: predictive factors of infection resolution
1263 and survival in patients treated with cefotaxime. Hepatology 17, 251–257.
1264 Tonkin-Hill, G., MacAlasdair, N., Ruis, C., Weimann, A., Horesh, G., Lees, J.A., Gladstone, R.A., Lo, S.,
1265 Beaudoin, C., Floto, R.A., Frost, S.D.W., Corander, J., Bentley, S.D., Parkhill, J., 2020. Producing
1266 polished prokaryotic pangenomes with the Panaroo pipeline. Genome Biology 21, 180.
1267 https://doi.org/10.1186/s13059-020-02090-4
1268 Tranah, T.H., Edwards, L.A., Schnabl, B., Shawcross, D.L., 2021. Targeting the gut-liver-immune axis
1269 to treat cirrhosis. Gut 70, 982–994. https://doi.org/10.1136/gutjnl-2020-320786
1270 Trebicka, J., Fernandez, J., Papp, M., Caraceni, P., Laleman, W., Gambino, C., Giovo, I., Uschner, F.E.,
1271 Jansen, C., Jimenez, C., Mookerjee, R., Gustot, T., Albillos, A., Bañares, R., Jarcuska, P., Steib,
1272 C., Reiberger, T., Acevedo, J., Gatti, P., Shawcross, D.L., Zeuzem, S., Zipprich, A., Piano, S., Berg,
1273 T., Bruns, T., Danielsen, K.V., Coenraad, M., Merli, M., Stauber, R., Zoller, H., Ramos, J.P., Solé,
1274 C., Soriano, G., de Gottardi, A., Gronbaek, H., Saliba, F., Trautwein, C., Kani, H.T., Francque, S.,
1275 Ryder, S., Nahon, P., Romero-Gomez, M., Van Vlierberghe, H., Francoz, C., Manns, M., Garcia-
1276 Lopez, E., Tufoni, M., Amoros, A., Pavesi, M., Sanchez, C., Praktiknjo, M., Curto, A., Pitarch, C.,

1277 Putignano, A., Moreno, E., Bernal, W., Aguilar, F., Clària, J., Ponzo, P., Vitalis, Z., Zaccherini, G.,
1278 Balogh, B., Gerbes, A., Vargas, V., Alessandria, C., Bernardi, M., Ginès, P., Moreau, R., Angeli,
1279 P., Jalan, R., Arroyo, V., PREDICT STUDY group of the EASL-CLIF CONSORTIUM, 2021. PREDICT
1280 identifies precipitating events associated with the clinical course of acutely decompensated
1281 cirrhosis. J Hepatol 74, 1097–1108. https://doi.org/10.1016/j.jhep.2020.11.019
1282 Trovato, F.M., Zia, R., Napoli, S., Wolfer, K., Huang, X., Morgan, P.E., Husbyn, H., Elgosbi, M.,
1283 Lucangeli, M., Miquel, R., Wilson, I., Heaton, N.D., Heneghan, M.A., Auzinger, G., Antoniades,
1284 C.G., Wendon, J.A., Patel, V.C., Coen, M., Triantafyllou, E., McPhail, M.J., 2021. Dysregulation
1285 of the Lysophosphatidylcholine/Autotaxin/Lysophosphatidic Acid Axis in Acute-on-Chronic
1286 Liver Failure Is Associated With Mortality and Systemic Inflammation by Lysophosphatidic
1287 Acid-Dependent Monocyte Activation. Hepatology 74, 907–925.
1288 https://doi.org/10.1002/hep.31738
1289 van den Berg, E.H., Flores-Guerrero, J.L., Garcia, E., Connelly, M.A., de Meijer, V.E., TransplantLines
1290 Investigators, Bakker, S.J.L., Blokzijl, H., Dullaart, R.P.F., 2023. High plasma levels of betaine,
1291 a trimethylamine N-Oxide-related metabolite, are associated with the severity of cirrhosis.
1292 Liver Int 43, 424–433. https://doi.org/10.1111/liv.15310
1293 Vergis, N., Atkinson, S.R., Knapp, S., Maurice, J., Allison, M., Austin, A., Forrest, E.H., Masson, S.,
1294 McCune, A., Patch, D., Richardson, P., Gleeson, D., Ryder, S.D., Wright, M., Thursz, M.R., 2017.
1295 In Patients With Severe Alcoholic Hepatitis, Prednisolone Increases Susceptibility to Infection
1296 and Infection-Related Mortality, and Is Associated With High Circulating Levels of Bacterial
1297 DNA. Gastroenterology 152, 1068-1077.e4. https://doi.org/10.1053/j.gastro.2016.12.019
1298 Vital, M., Rud, T., Rath, S., Pieper, D.H., Schlüter, D., 2019. Diversity of Bacteria Exhibiting Bile Acid-
1299 inducible 7α-dehydroxylation Genes in the Human Gut. Comput Struct Biotechnol J 17, 1016–
1300 1019. https://doi.org/10.1016/j.csbj.2019.07.012
1301 Walker, B.J., Abeel, T., Shea, T., Priest, M., Abouelliel, A., Sakthikumar, S., Cuomo, C.A., Zeng, Q.,
1302 Wortman, J., Young, S.K., Earl, A.M., 2014. Pilon: An Integrated Tool for Comprehensive
1303 Microbial Variant Detection and Genome Assembly Improvement. PLOS ONE 9, e112963.
1304 https://doi.org/10.1371/journal.pone.0112963
1305 Wang, Q., Chen, C., Zuo, S., Cao, K., Li, H., 2023. Integrative analysis of the gut microbiota and faecal
1306 and serum short-chain fatty acids and tryptophan metabolites in patients with cirrhosis and
1307 hepatic encephalopathy. J Transl Med 21, 395. https://doi.org/10.1186/s12967-023-04262-9
1308 Wick, R.R., Judd, L.M., Gorrie, C.L., Holt, K.E., 2017. Unicycler: Resolving bacterial genome assemblies
1309 from short and long sequencing reads. PLOS Computational Biology 13, e1005595.
1310 https://doi.org/10.1371/journal.pcbi.1005595
1311 Williams, H.R.T., Cox, I.J., Walker, D.G., Cobbold, J.F.L., Taylor-Robinson, S.D., Marshall, S.E., Orchard,
1312 T.R., 2010. Differences in gut microbial metabolism are responsible for reduced hippurate
1313 synthesis in Crohn's disease. BMC Gastroenterol 10, 108. https://doi.org/10.1186/1471-
1314 230X-10-108
1315 Wong, F., Piano, S., Singh, V., Bartoletti, M., Maiwall, R., Alessandria, C., Fernandez, J., Soares, E.C.,
1316 Kim, D.J., Kim, S.E., Marino, M., Vorobioff, J., Barea, R. de C.R., Merli, M., Elkrief, L., Vargas,
1317 V., Krag, A., Singh, S.P., Lesmana, L.A., Toledo, C., Marciano, S., Verhelst, X., Intagliata, N.,
1318 Rabinowich, L., Colombato, L., Kim, S.G., Gerbes, A., Durand, F., Roblero, J.P., Bruns, T., Yoon,
1319 E.L., Girala, M., Pyrsopoulos, N.T., Kim, T.H., Yim, S.Y., Juanola, A., Gadano, A., Angeli, P.,
1320 International Club of Ascites Global Study Group, 2021. Clinical features and evolution of

1321 bacterial infection-related acute-on-chronic liver failure. J Hepatol 74, 330–339.
1322 https://doi.org/10.1016/j.jhep.2020.07.046
1323 Y, Furusawa, Y, O., S, F., Ta, E., G, N., D, T., Y, N., C, U., K, K., T, K., M, Takahashi, Nn, F., S, M., E, M., S,
1324 Hino, K, A., S, O., Y, Fujimura, T, L., Jm, C., Dl, T., M, Tomita, S, Hori, O, O., T, M., H, K., J, K., K,
1325 Honda, K, Hase, H, O., 2013. Commensal microbe-derived butyrate induces the differentiation
1326 of colonic regulatory T cells. Nature 504. https://doi.org/10.1038/nature12721
1327 Zapun, A., Contreras-Martel, C., Vernet, T., 2008. Penicillin-binding proteins and beta-lactam
1328 resistance. FEMS microbiology reviews 32. https://doi.org/10.1111/j.1574-
1329 6976.2007.00095.x
1330 Zhang, J., Kobert, K., Flouri, T., Stamatakis, A., 2014. PEAR: a fast and accurate Illumina Paired-End
1331 reAd mergeR. Bioinformatics 30, 614–620. https://doi.org/10.1093/bioinformatics/btt593
1332 Zhang, X., Bierschenk, D., Top, J., Anastasiou, I., Bonten, M.J., Willems, R.J., van Schaik, W., 2013.
1333 Functional genomic analysis of bile salt resistance in Enterococcus faecium. BMC Genomics
1334 14, 299. https://doi.org/10.1186/1471-2164-14-299
1335 Zimmermann, P., Curtis, N., 2019. The effect of antibiotics on the composition of the intestinal
1336 microbiota - a systematic review. The Journal of infection 79.
1337 https://doi.org/10.1016/j.jinf.2019.10.008

1338

1339

1340 **Table 1**: Summary of clinical characteristics of patient and healthy participant study groups (all values given as median [IQR]). **Statistics:**
1341 Statistical analyses were performed using GraphPad Prism, version 10.3.1 (San Diego, USA). Data are presented as medians with interquartile
1342 ranges [IQRs] or as counts with percentages [%]. Continuous data were analysed with the Mann-Whitney test or Kruskal-Wallis test, as
1343 appropriate. Comparisons between categorical data were conducted using the chi-square or Fisher's exact test, as appropriate.

1344

Parameters			HC (n=40)	SC (n=15)	DC (n=81)	ACLF (n=57)	P value
General	Age (years)		36 (32-41)	59 (54-69)	55 (49-61)	49 (42-59)	<0.0001
	Male gender (n (%))		20 (50%)	11 (73.3%)	52 (64.2%)	36 (63.2%)	0.3287
	BMI (kg/m^2)		N/A	27.2 (23.5-32.6)	27.4 (24.0-30.5)	22.7 (20.8-23.2)	<0.0001
Aetiology of cirrhosis	Alcohol-related liver disease (ARLD) (n (%))		N/A	9 (60.0%)	57 (70.4%)	33 (57.9%)	0.2950
	Drinking/ Abstinent in ARLD	Alcohol actively drinking (n (%))	N/A	0	12 (21.0%)	19 (57.6%)	0.0002
		Alcohol abstinent (n (%))	N/A	9 (100%)	45 (79.0%)	14 (42.4%)	
	Metabolic dysfunction-associated steatotic liver disease (MASLD) (n (%))		N/A	3 (20.0%)	7 (8.6%)	6 (10.5%)	0.4181

1

	Cholestatic/autoimmune (n (%)): Primary biliary cholangitis (PBC), primary sclerosing cholangitis (PSC), Alagille syndrome, biliary atresia, and autoimmune hepatitis (AIH)		N/A	1 (6.7%)	6 (7.4%)	11 (19.3%)	0.0832
	Metabolic (number (%)): Wilson's disease, haemochromatosis and alpha-1-antitrypsin (A1AT) deficiency		N/A	1 (6.7%)	5 (6.2%)	3 (5.3%)	0.9663
	Other (n (%)): 'Cryptogenic', treated viral hepatitis, chronic veno-occlusive related-cirrhosis (Budd Chiari), chronic porto-mesenteric venous insufficiency cirrhosis, and drug induced		N/A	1 (6.7%)	6 (7.4%)	4 (7%)	0.9928
Clinical features at enrolment	Temperature (°C)		N/A	36.5 (36.3-37.2)	36.7 (36.4-37.0)	36.5 (36.1-37.1)	0.2121
	Ascites present (n (%))		N/A	5 (33.3%)	58 (71.6%)	55 (96.5%)	<0.0001
	Ascites grade (n (%))	Small	N/A	5 (100%)	25 (43.1%)	35 (63.6%)	0.0107
		Moderate / Severe	N/A	0	33 (56.9%)	20 (36.4%)	
	Hepatic encephalopathy present (n (%))		N/A	1 (6.7%)	35 (43.2%)	49 (86.0%)	<0.0001
		1-2	N/A	1 (100%)	35 (100%)	24 (49.0%)	<0.0001

	Hepatic encephalopathy grade	3-4	N/A	0	0	25 (51.0%)	
	Mean arterial pressure (mmHg)		N/A	95 (87-100)	81 (76-89)	75 (70-82)	<0.0001
	Presence of bacterial infection (n (%))	Blood culture	N/A	0	2 (2.5%)	3 (5.3%)	0.4996
		Urine culture	N/A	0	5 (6.2%)	2 (3.5%)	0.5114
	Heart rate (beats per minute)		N/A	76 (65-82)	77 (60-88)	87 (78-95)	0.0010
Antibacterial therapy at enrolment (number (%))	Antibiotics – any		N/A	3 (20%)	37 (45.7%)	52 (91.2%)	<0.0001
	Antifungal – any		N/A	0	2 (2.4%)	20 (35.1%)	<0.0001
	Rifaximin		N/A	1 (6.7%)	10 (12.4%)	2 (3.5%)	0.2583
	Fluoroquinolone (Norfloxacin, Ciprofloxacin)		N/A	0	8 (9.9%)	0	0.0702
Other pharmacotherapy at enrolment (number (%))	Proton pump inhibitors (Omeprazole, Lansoprazole)		N/A	10 (66.7%)	44 (54.3%)	36 (63.2%)	0.4721
	Lactulose		N/A	2 (13.3%)	30 (37.0%)	2 (3.5%)	0.1234
	Non-selective beta-blockers (Propranolol, Carvedilol)		N/A	6 (40%)	34 (42.0%)	14 (24.6%)	0.1001

	H2 antagonist (Ranitidine)	N/A	0	3 (3.7%)	0	0.2567
Laboratory parameters	Haemoglobin (g/dl)	N/A	130 ± 25	112 ± 21	92 ± 15	<0.0001
	Leukocyte count (x10^9/L)	N/A	4.46 (3.96-6.11)	5.57 (4.25-7.39)	9.74 (6.54-14.57)	<0.0001
	Neutrophils (x10^9/L)	N/A	2.92 (2.14-3.69)	3.70 (2.37-5.29)	7.70 (4.85-12.21)	<0.0001
	Platelet count (x10^9/L)	N/A	111 (99-151)	106 (75-165)	86 (56-115)	0.0061
	INR	N/A	1.15 (1.10-1.29)	1.44 (1.29-1.75)	2.09 (1.69-2.93)	<0.0001
	Serum creatinine (µmol/L)	N/A	73 (66-84)	77 (57-94)	135 (87-206)	<0.0001
	Serum bilirubin (µmol/L)	N/A	20 (11-25)	41 (24-72)	209 (84-371)	<0.0001
	Albumin (g/L)	N/A	39 ± 4	33 ± 6	27 ± 7	<0.0001
	C-reactive protein (mg/L)	N/A	5.5 (2.3-11.1)	11.7 (3.4-32.9)	47.3 (23.7-70.7)	<0.0001
	Blood lactate (mmol/L)	N/A	1.4 (1.2-1.9)	1.5 (1.2-2.1)	2 (1.6-3.2)	0.0006
	Venous ammonia (µmol/L)	N/A	61 (28-88)	53 (33-72)	68 (47-107)	0.0710
Disease severity & prognostic scores	Child Pugh	N/A	6 (5-6)	8 (8-10)	12 (11-13)	<0.0001
	MELD	N/A	9 (8-11)	16 (12-23)	34 (29-39)	<0.0001
	UKELD	N/A	49 ± 3	55 ± 5	61 ± 6	<0.0001
	CLIF-C-AD	N/A	N/A	49 (43-53)	N/A	—

	CLIF-C-ACLF	N/A	N/A	N/A	54 (46-66)	—
	CLIF-OF	N/A	N/A	7 (6-8)	13 (11-15)	<0.0001
Transplant-free survival	30-day	N/A	0	72 (88.9%)	24 (42.1%)	<0.0001
	90-day	N/A	0	63 (77.8%))	14 (24.6%)	<0.0001

1345

1346 # 7. Supplementary data

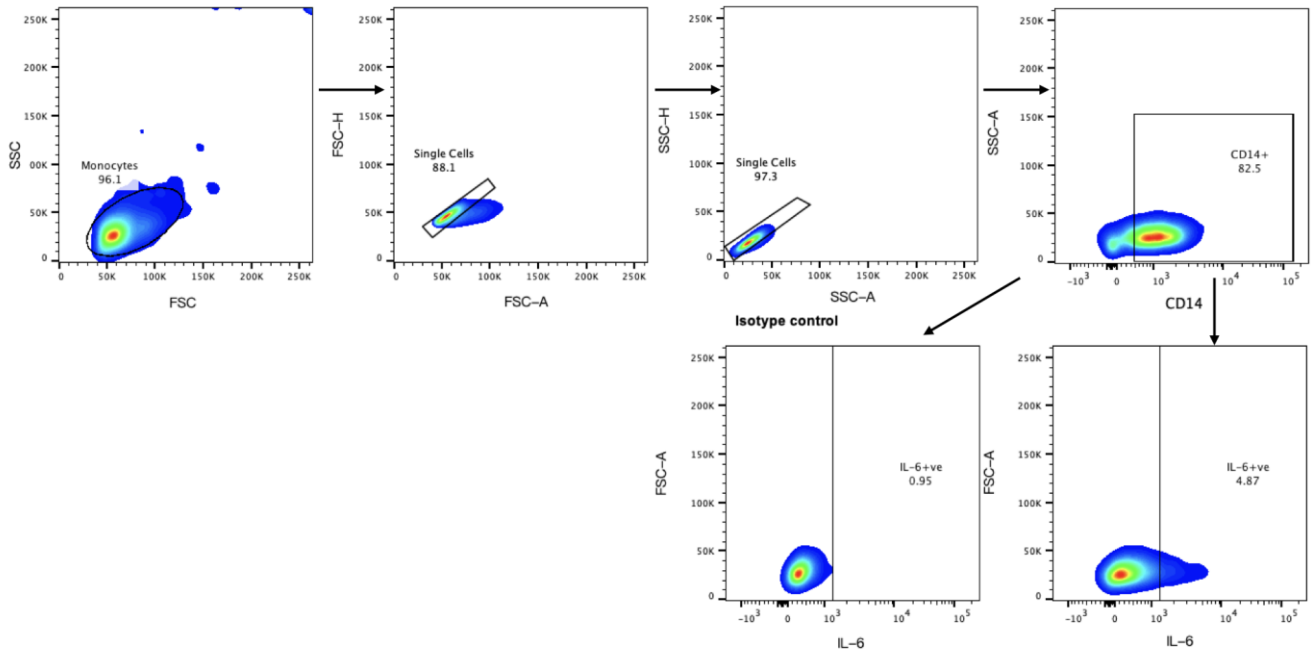

1347

1348 **Supplementary Figure 1.** Representative FACS gating strategy used to identify CD14+ monocytes in
1349 peripheral blood mononuclear cells (PBMCs) with isotype control used to determine the IL-6-
1350 producing monocytes (%) in response to LPS stimulation. Side scatter (SSC), forward scatter (FSC).

1351

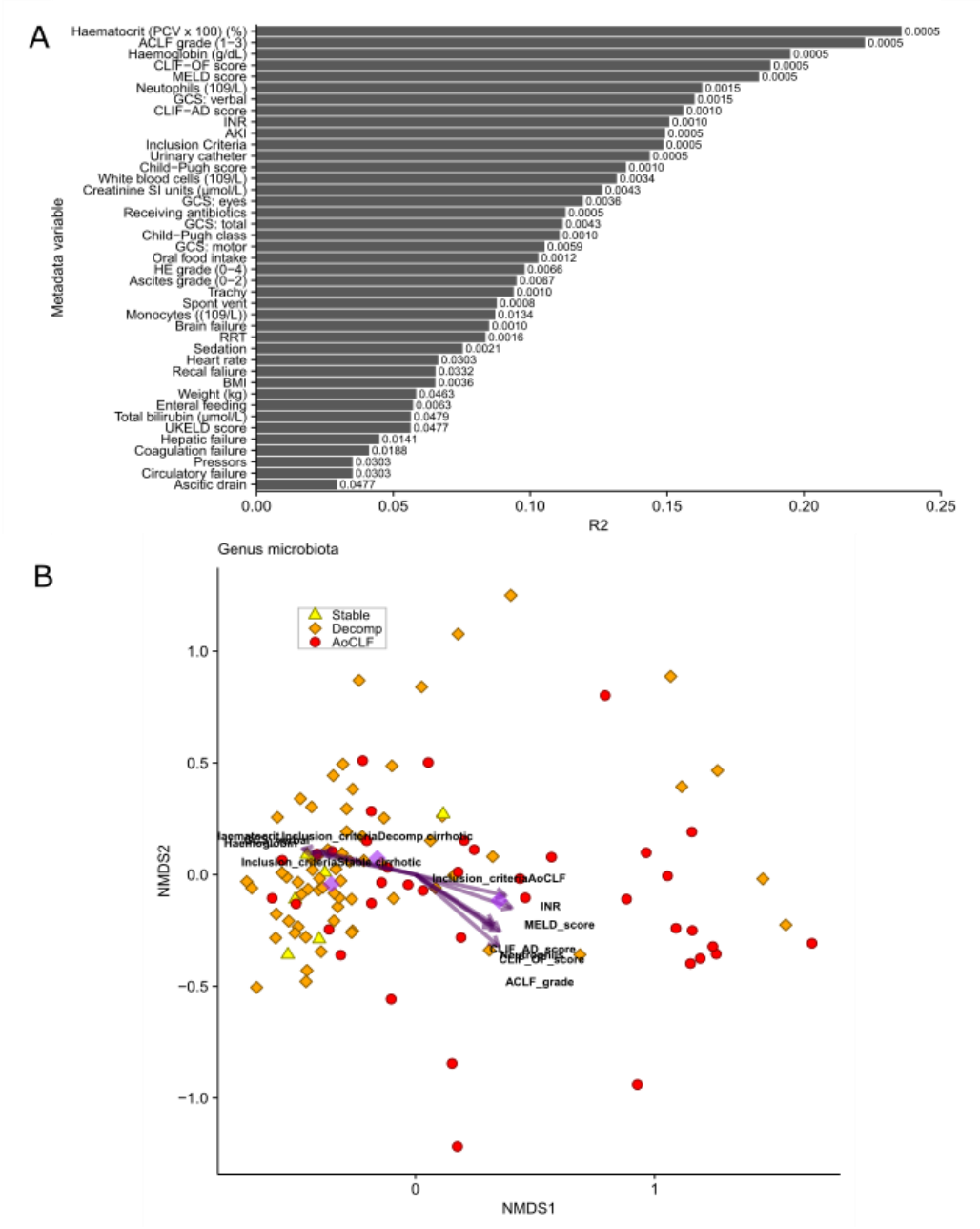

Supplementary Figure 2. Clinical metadata associated with cirrhosis patient gut microbiota composition.

(A) Results of envfit analysis showing clinical metadata variables significantly associated with microbiota composition after correction for multiple testing using False Discovery Rate. Bars show the R2 (squared correlation coefficient) of the correlation and numbers on bars show adjusted P-values. (B) NMDS ordination plot showing gut microbiota composition of individual liver patients with the ten clinical metadata variables with the highest R2 overlayed.

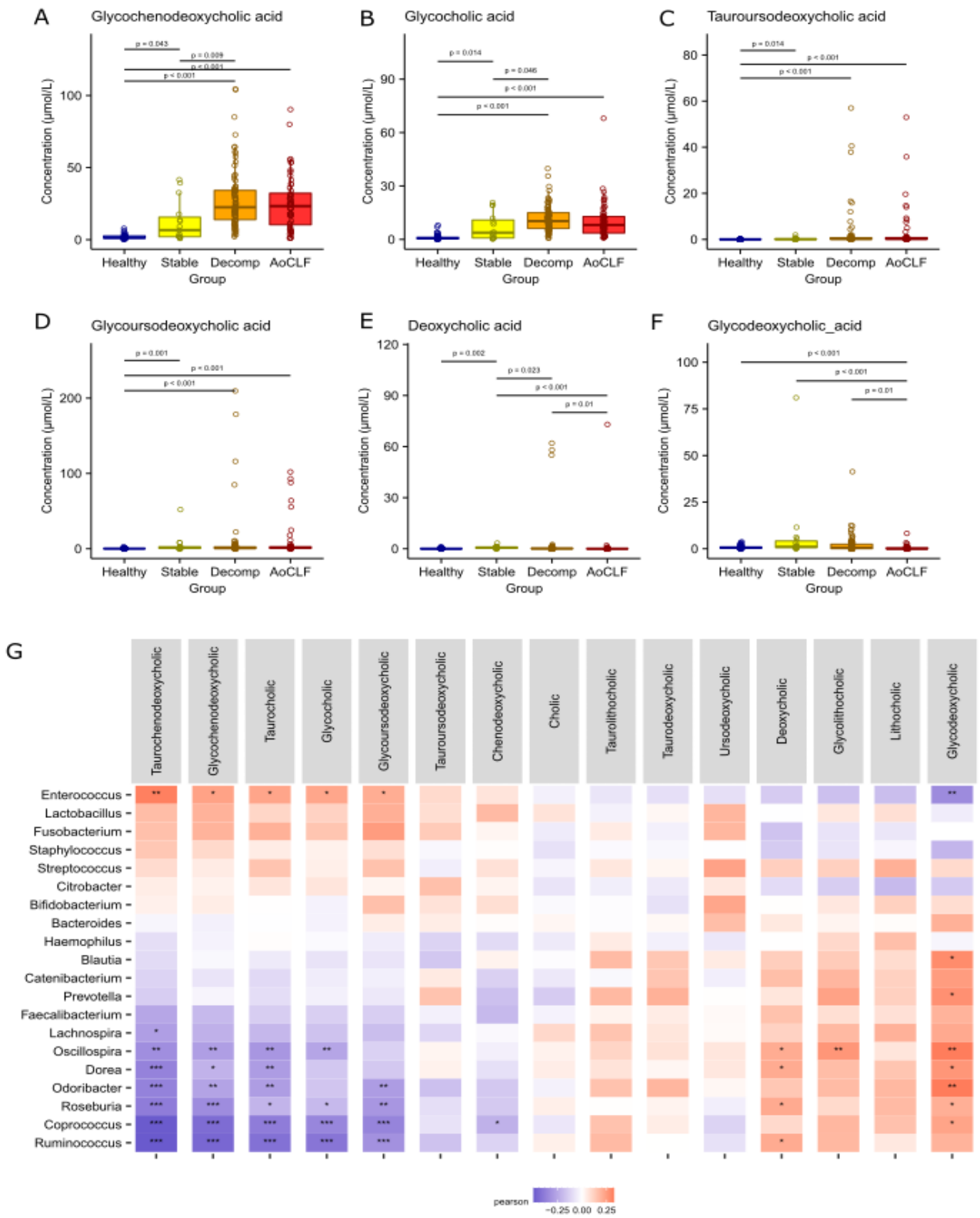

1360

1361 **Supplementary Figure 3**. Individual bile acid concentrations by cirrhosis severity and correlations

1362 between genus proportion and bile acids.

1363 (A) Glycochenodeoxycholic acid, (B) Glycocholic acid, (C) Tauroursodeoxycholic acid, (D)
1364 Glycoursodeoxycholic acid, (E) Deoxycholic acid, (F) Glycodeoxycholic acid, (F) Pearson correlations
1365 between normalised plasma bile acid concentrations and normalised genus relative abundance using
1366 a Pearson correlation. P-value: * = $p<0.05$, ** = $p<0.01$, ** = $p<0.001$. Significance corrected for
1367 multiple testing.

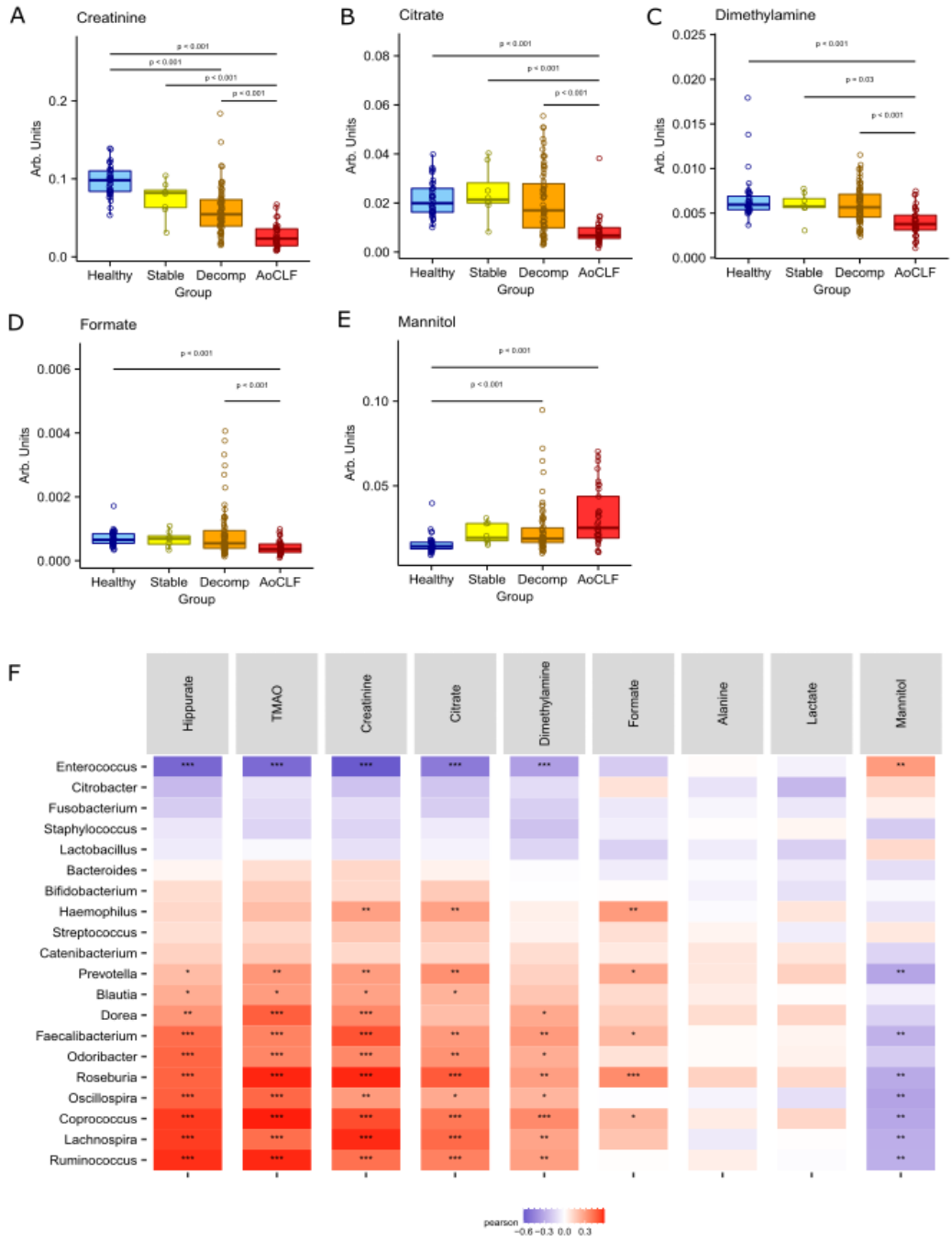

1368

1369 **Supplementary Figure 4**. Individual urinary metabolites by cirrhosis severity and correlations
1370 between genus proportion and plasma metabolites.

1371 (A) Creatinine, (B) Citrate, (C) Dimethylamine, (D) Formate, (E) Mannitol, (F) Correlations between
1372 normalised urinary metabolites and normalised genus relative abundance using a Pearson
1373 correlation. P-value: * = p<0.05, ** = p<0.01, ** = p<0.001. Significance corrected for multiple testing.

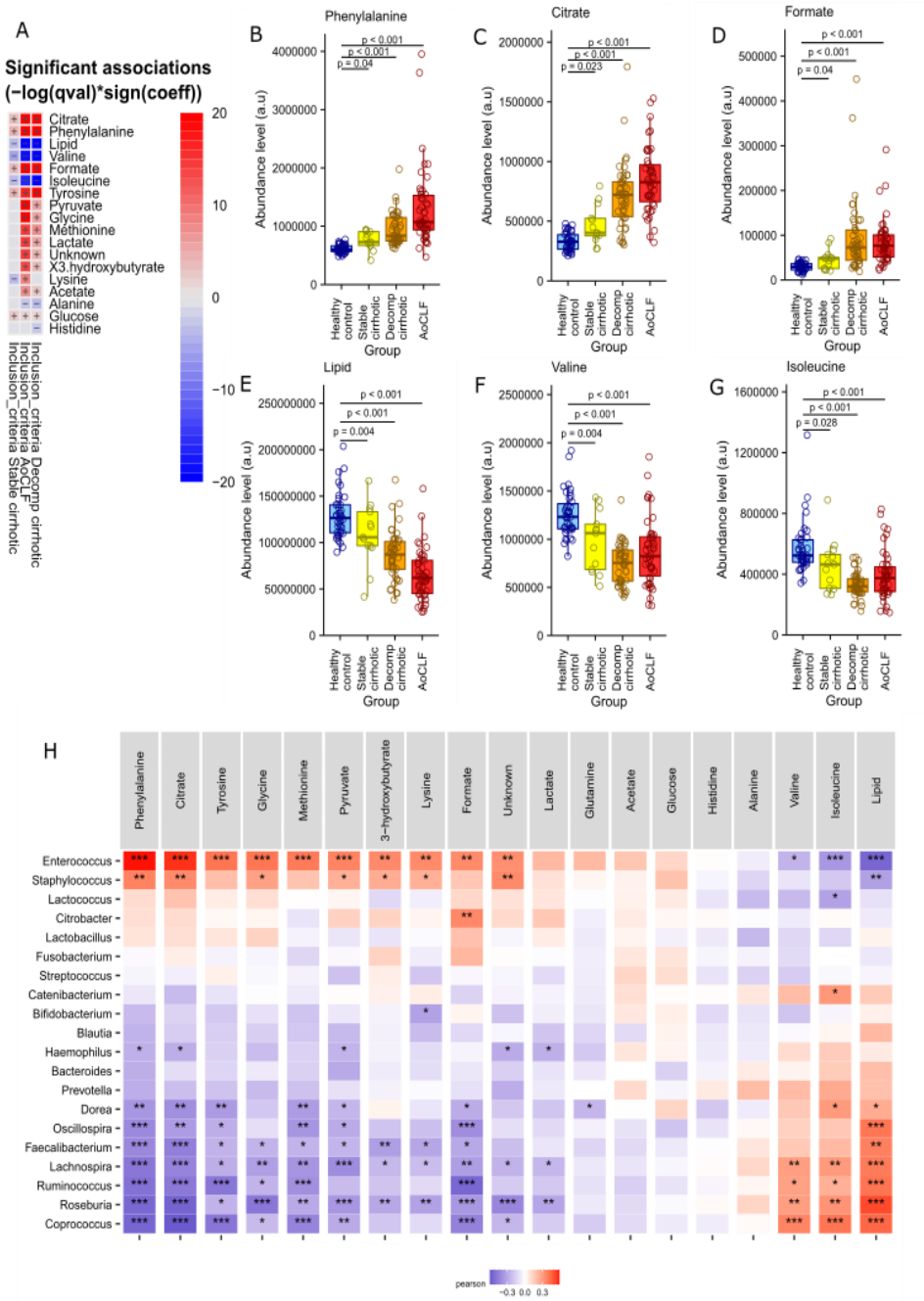

Supplementary Figure 5. Individual plasma metabolites by cirrhosis severity and correlations between genus proportion and plasma metabolites.

(A) Phenylalanine, (B) Citrate, (C) Formate, (D) Lipid, (E) Valine, (F) Isoleucine, (G) Correlations between normalised plasma metabolites and normalised genus relative abundance using a Pearson correlation. P-value: * = p<0.05, ** = p<0.01, *** = p<0.001. Significance corrected for multiple testing.

1381

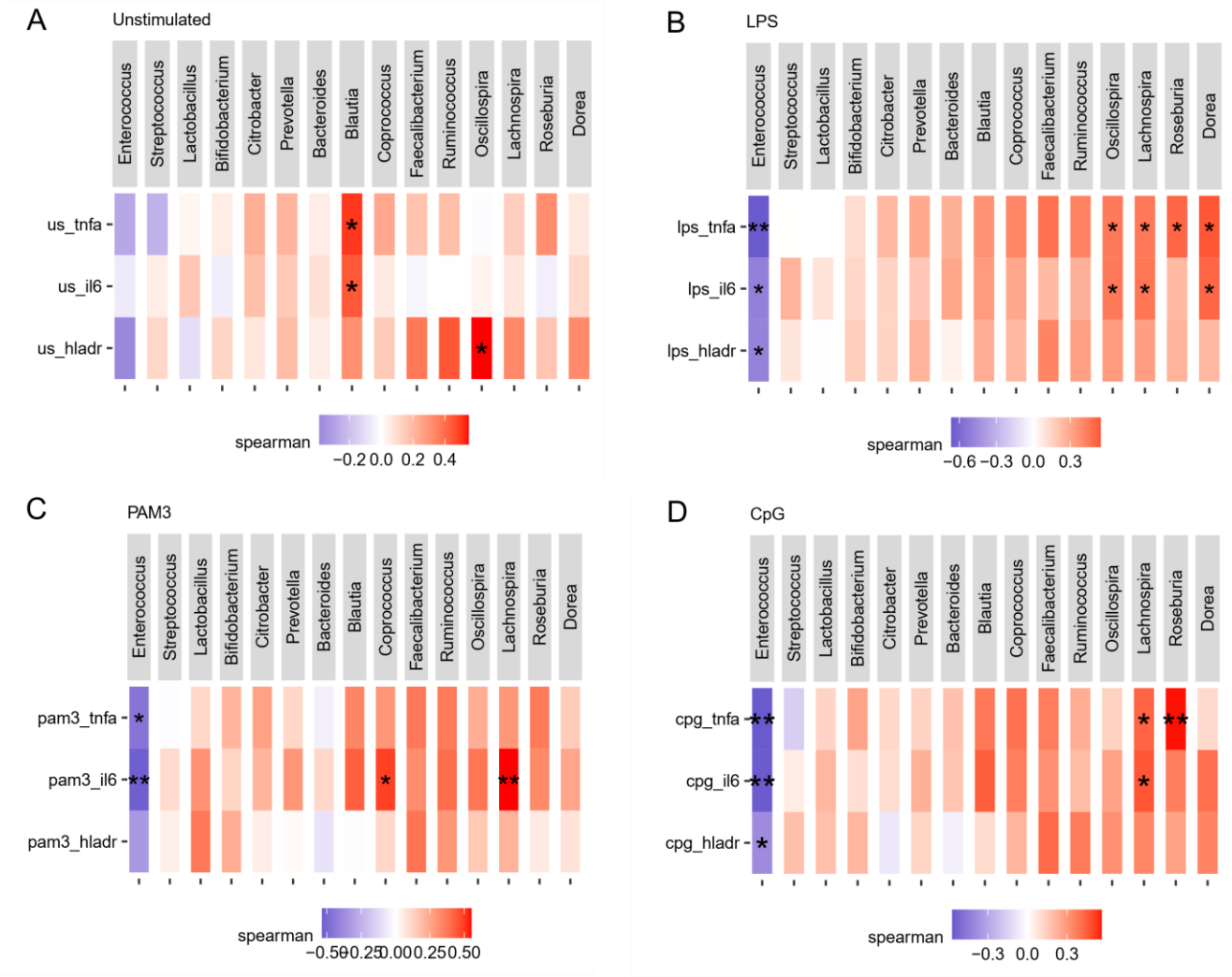

1382

1383 **Supplementary Figure 6**. Correlations between genus proportion and monocyte stimulation.

1384 Full correlations between the top 15 most abundant genera and TNF-alpha, IL-6, and HLA-DR
1385 percentage in (A) Unstimulated, (B) LPS stimulated, (C) PAM3 stimulated, and (D) CpG simulated
1386 monocytes. Correlations between normalised plasma metabolites and normalised genus relative
1387 abundance using a Pearson correlation. P-value: * = $p<0.05$, ** = $p<0.01$. Significance corrected for
1388 multiple testing.

1389

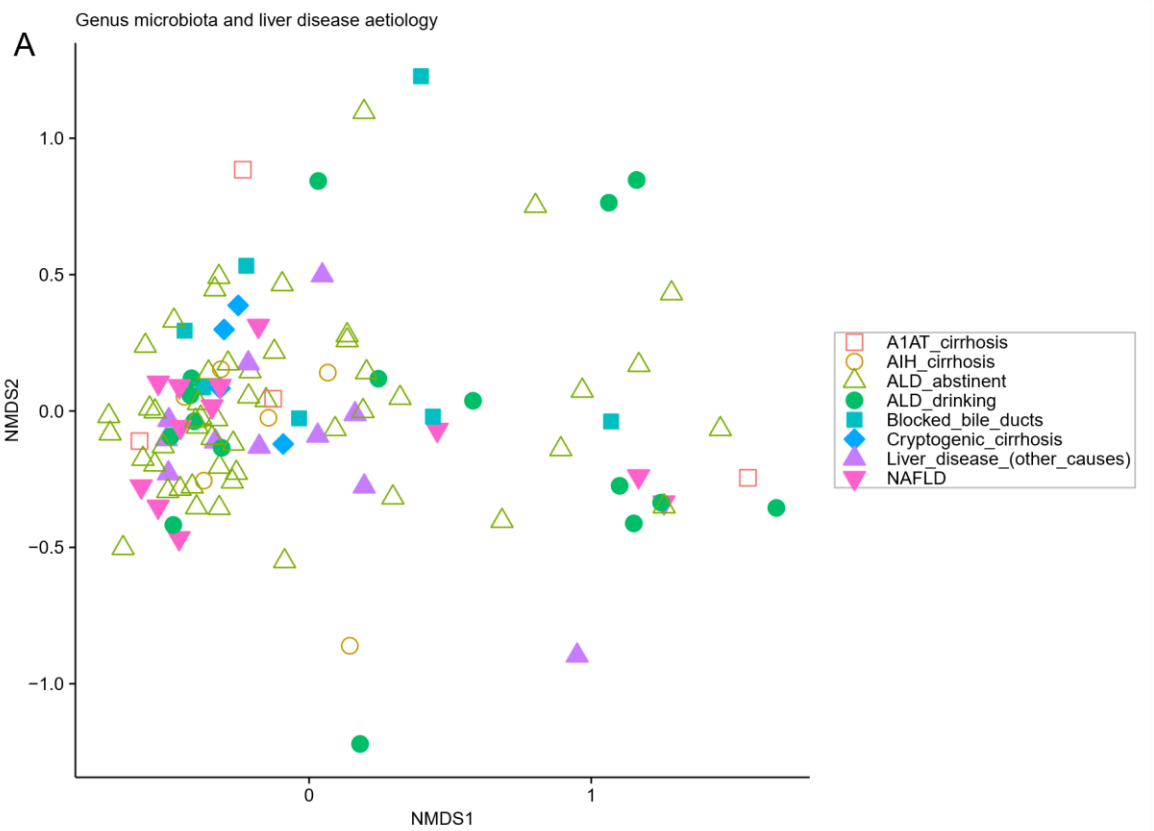

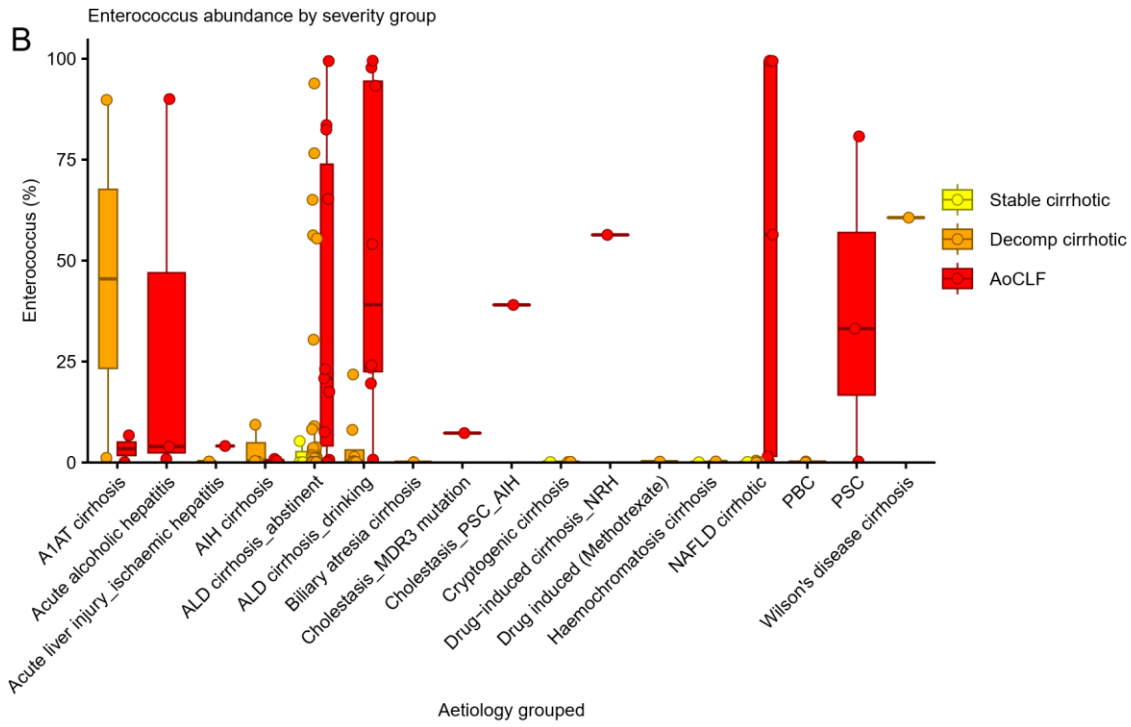

Supplementary Figure 7. Aetiology associations with overall microbiota composition and *Enterococcus* abundance.

1393 (A) NMDS clustering of overall genus level faecal microbiota composition based on a Bray-Curtis
1394 matrix showing patient samples with patient aetiology condensed to eight groups for the purposes
1395 of analysis showing a lack of clustering by aetiology (PERMANOVA: P = 0.1). (B) Box plots show full
1396 patient aetiology groups with faecal *Enterococcus* abundance grouped by illness severity.